

Tanycytic networks mediate energy balance by feeding lactate to glucose-insensitive POMC neurons

Tori Lhomme, Jerome Clasadonte, Monica Imbernon 1&, Daniela Fernandois, Florent Sauve, Emilie Caron, Natalia da Silva Lima, Violeta Heras, Ines Martinez-Corral, Helge Mueller-Fielitz, et al.

▶ **To cite this version:**

Tori Lhomme, Jerome Clasadonte, Monica Imbernon 1&, Daniela Fernandois, Florent Sauve, et al.. Tanycytic networks mediate energy balance by feeding lactate to glucose-insensitive POMC neurons. Journal of Clinical Investigation, 2021, Online ahead of print. inserm-03306217

HAL Id: inserm-03306217

https://inserm.hal.science/inserm-03306217

Submitted on 29 Jul 2021

HAL is a multi-disciplinary open access archive for the deposit and dissemination of scientific research documents, whether they are published or not. The documents may come from teaching and research institutions in France or abroad, or from public or private research centers.

L'archive ouverte pluridisciplinaire **HAL**, est destinée au dépôt et à la diffusion de documents scientifiques de niveau recherche, publiés ou non, émanant des établissements d'enseignement et de recherche français ou étrangers, des laboratoires publics ou privés.

The Journal of Clinical Investigation
Reference: 140521-JCI-RG-RV-2

Tanycytic networks mediate energy balance by feeding lactate to glucose-insensitive POMC neurons

Tori Lhomme[1], Jerome Clasadonte[1&], Monica Imbernon[1&], Daniela Fernandois[1&], Florent Sauve[1], Emilie Caron[1], Natalia da Silva Lima[2,3], Violeta Heras[2,3], Ines Martinez-Corral[1], Helge Mueller-Fielitz[4], S. Rasika[1], Markus Schwaninger[4§], Ruben Nogueiras[2,3§], Vincent Prevot[1§*]

[1] Univ. Lille, Inserm, CHU Lille, Laboratory of Development and Plasticity of the Neuroendocrine Brain, Lille Neuroscience & Cognition, UMR-S 1172, EGID and DISTALZ, F-59000 Lille, France
[2] CIMUS, Universidade de Santiago de Compostela-Instituto de Investigación Sanitaria, Santiago de Compostela, 15782, Spain
[3] CIBER Fisiopatología de la Obesidad y Nutrición (CIBERobn), 15706, Spain
[4] Institute for Experimental and Clinical Pharmacology and Toxicology, University of Lübeck, Lübeck, Germany
[&] These authors equally contributed to this work
[§] These authors jointly supervised this work

Running head: Tanycyte-neuron metabolic interactions

Number of words (abstract): 150
Number of words (text): 11899
Number of figures: 5
Number of Supplementary Figures: 6
Number of Supplementary tables: 1

Corresponding author: Vincent Prevot, Ph.D., Inserm U1172, Bâtiment Biserte, Place de Verdun, 59045 Lille Cedex, France
Tel: +33 320-62-20-64
Fax: +33 320-53-85-62
E-mail: vincent.prevot@inserm.fr

CONFLICT OF INTEREST STATMENT

The authors declare no competing interest.

ABSTRACT

Hypothalamic glucose sensing enables an organism to match energy expenditure and food intake to circulating levels of glucose, the main energy source of the brain. Here, we established that tanycytes of the hypothalamic arcuate nucleus, specialized glia that line the wall of the third ventricle, convert brain glucose supplies into lactate that they transmit through monocarboxylate transporters to arcuate proopiomelanocortin neurons, which integrate this signal to drive their activity and to adapt the metabolic response to meet physiological demands. Furthermore, this transmission required the formation of extensive Connexin-43 gap-junction-mediated metabolic networks by arcuate tanycytes. Selectively suppressing either tanycytic monocarboxylate transporters or gap junctions resulted in altered feeding behavior and energy metabolism. Tanycytic intercellular communication and lactate production are thus integral to the mechanism by which hypothalamic neurons that regulate energy and glucose homeostasis efficiently perceive alterations in systemic glucose levels as a function of the physiological state of the organism.

INTRODUCTION

Glucose plays a dual role in the brain: it is both an essential fuel that sustains brain activity, and an indicator of peripheral energy status. Circulating glucose levels fluctuate as a function of food intake or energy expenditure. However, the entrance of glucose into the brain is regulated by specific transport systems (1, 2) that ensure that extracellular glucose concentrations in the brain (~ 2 mM), while significantly lower than those in the blood (~ 5 mM), remain constant to fulfill the energy needs of brain cells, regardless of the physiological state of the individual (3). How then do brain networks whose function it is to maintain energy homeostasis by modulating metabolic pathways detect changes in peripheral energy status? The arcuate nucleus of the hypothalamus (ARH), which flanks the third ventricle (3V) on both sides, contains discrete populations of neurons that are critically involved in the regulation of energy homeostasis (4, 5). Among them, the pro-opiomelanocortin (POMC) neurons (6, 7), which are electrically excited by glucose, are well placed to adjust food intake and energy expenditure in response to changes in circulating glucose levels (8). However, whether POMC neurons are themselves capable of sensing glucose remains controversial (9, 10). Instead, it seems logical for this role to be assumed by a different class of cells that is in touch on the one hand with both the blood and the cerebrospinal fluid (CSF), whose glucose concentrations vary in proportion to blood concentrations (11, 12), and on the other hand with POMC neurons, and that can therefore transmit changes in glucose levels in these two compartments or translate them into a signal that the neurons can perceive.

Here, we thus test the hypothesis that POMC neuronal activity is not directly controlled by glucose but by its metabolite lactate (13), and ask whether tanycytes, peculiar glial cells constituting a CSF-brain barrier along the wall of the third ventricle that replaces the traditional blood-brain barrier (14, 15), act as the source of the metabolic signal required by POMC neurons for hypothalamic glucose sensing and the control of energy homeostasis.

RESULTS

POMC neurons use lactate and not glucose as an energy substrate

Many glucose-sensing neurons respond to or integrate signals from glucose metabolites, especially lactate (10). To determine whether POMC neurons also use lactate as an energy substrate, we used whole-cell current-clamp recordings in acute brain slices from *tdTomato*^{POMC} mice (Figure 1A). In the presence of physiological levels of glucose (2.5 mM), POMC neurons exhibited tonic firing. However, the bath application of a selective blocker of the monocarboxylate transporters (MCTs), α-cyano-4-hydroxycinnamate (4-CIN, 500 μM), to block lactate influx into cells (16), completely inhibited this tonic firing (Wilcoxon matched-pair test, *P*=0.0078, 8 cells, 5 mice) (Figure 1B and 1C), indicating that lactate and not glucose was fueling POMC neuronal activity. We next induced glucose deprivation by switching from 2.5 mM to 0 mM glucose in artificial cerebrospinal fluid (ACSF), which caused a marked decrease in POMC neuron firing (one-way repeated measures ANOVA followed by Tukey's post hoc test, *P*=0.0015, 6 cells, 4 mice). The bath application of 5 mM lactate (equicaloric to 2.5 mM glucose) (16) restored the spontaneous firing frequency of glucose-deprived POMC neurons (*P*=0.0280, 6 cells, 4 mice) (Figure 1D and 1E). This rescue effect was in turn abolished by the bath application of 10 mM oxamate (one-way repeated measures ANOVA followed by Tukey's post hoc test, *P*=0.0277, 7 cells, 5 mice) (Figure 1F-1I), which inhibits lactate dehydrogenase (LDH), an enzyme responsible for the conversion of lactate to pyruvate, the metabolite that principally fuels neurons through its entry into the tricarboxylic acid cycle (17). In accordance with this sequence of events, while the addition of lactate did not compensate for the loss of neuronal activity induced by oxamate (one-way repeated measures ANOVA followed by Tukey's post hoc test, *P*=0.7811, 5 cells, 4 mice) (Figure 1F and 1G), the bath application of pyruvate completely reversed it (5 mM) (one-way repeated measures ANOVA followed by Tukey's post hoc test, *P*=0.046, 7 cells, 5 mice) (Figure 1H and 1I). To ascertain that changes in POMC neuronal activity were not due to an indirect action of oxamate on neighboring neurons, oxamate was directly delivered into the cytoplasm of the recorded cell via the patch pipette (Figure 1J). This cell-restricted LDH inhibition also blunted neuronal activity (one-way repeated measures ANOVA followed by Tukey's post hoc test, *P*=0.0236, 7 cells, 5 mice) in a pyruvate-reversible manner (*P*=0.0145, 7 cells, 5 mice) (Figure 1J and 1K). Altogether, these results suggest that rather than glucose, lactate produced locally from glucose in living brain slices is taken up by POMC neurons via MCTs, and sustains their neuronal activity through its conversion to pyruvate.

Tanycytes shuttle lactate to POMC neurons

ARH tanycytes, thanks to the position of their cell bodies lining the walls of the third ventricle and end-feet that contact vessels of the blood-brain barrier (14), are in contact with both blood-borne and CSF-borne glucose and also express glucose-sensing machinery reminiscent of that found in pancreatic β-cells (18-20). In addition, tanycytes express functional MCTs (21, 22). To determine whether, rather than the astrocytic lactate shuttle that feeds neuronal activity in other brain areas (23, 24), tanycytes could be the source of the endogenous lactate required by POMC neurons, we first performed experiments in primary cultures of tanycytes, which we have previously extensively characterized (25, 26). Immunofluorescence experiments showed that cultured tanycytes expressed the lactate transporters Mct1 and Mct4 (Figure 2A and 2B). In addition, the spontaneous lactate release seen from tanycytes cultured in glucose-containing serum-free defined medium (Figure 2C) was blunted by the addition into the culture medium of the non-metabolizable glucose analog 2-deoxyglucose (2-DG, 50 mM) (ordinary one-way ANOVA followed by Tukey's post hoc test, P=0.0016, n=5) (Figure 2C), which also blunted lactate production within the cells (ordinary one-way ANOVA followed by Tukey's post hoc test, P<0.0001, n=5) (Figure 2D). Since Mcts are responsible for lactate exit from cells, inhibiting tanycytic Mcts by treating the cultures for 30 min with 500 μM 4-CIN abrogated the ability of tanycytes to release lactate (P=0.012, n=6) (Figure 2C), and caused an accumulation of lactate in their cytoplasm (P<0.0001, n=6) (Figure 2D). These *in vitro* results indicate that tanycytes could indeed produce and release lactate through their uptake and metabolization of glucose.

Next, to test the possibility that lactate released by tanycytes fuels POMC neurons in the ARH, we asked whether the delivery of lactate into ARH tanycytes could rescue activity in POMC neurons during glucose deprivation in living brain slices. A single tanycyte was dialyzed with 5 mM lactate while performing whole-cell recording from a distant POMC neuron (50-200 μm apart; Figure S1A-S1C, Figure 2E-2J). When the tanycyte was dialyzed with lactate, the reduction in action potential firing seen with glucose deprivation in Figure 1D no longer occurred (one-way repeated measures ANOVA followed by Tukey's post hoc test, P=0.9974, 6 cells, 5 mice) (Figure 2H and 2I); this was true of all the POMC neurons patched (n=9; including some not shown), even when they were considerably removed from the patched tanycyte and not in the path of the tanycytic process (Figure 2J). This tanycyte-mediated rescue of POMC neuronal firing was reversed with the loss of the tanycytic patch that sometimes occurred during the course of the experiment (Figure S1D), but could be counteracted by bath application of 5 mM lactate

(Figure S1D) as shown in Figure 1D. We next explored whether selectively blocking lactate production in the patched tanycytes would have an impact on the activity of the POMC neurons with which they are connected, regardless of the presence of physiological levels of glucose (2.5 mM) (Figure 2K). When a single tanycyte was dialyzed with the LDH inhibitor, oxamate, to block the conversion of pyruvate to lactate, it induced a drastic reduction in action potential firing in the paired POMC neuron (one-way repeated measures ANOVA followed by Tukey's post hoc test, *P*=0.0143, 6 cells, 5 mice), an effect that was rescued by bath application of lactate (*P*=0.0474, 6 cells, 5 mice) (Figure 2L-2N). Altogether, these results suggest that tanycytes metabolize glucose into lactate for delivery to the POMC neurons with which they are functionally connected, and that this tanycytic lactate production is both necessary and sufficient for the tonic firing of POMC neurons. In addition, the rescue of POMC neuronal activity by tanycyte-delivered lactate was completely suppressed by 4-CIN (*P*=0.0288, 6 cells, 5 mice) (500 μM; Figure 2H-2I), indicating that lactate transport through MCTs is required for this effect.

Mct1 and Mct4 expression by tanycytes is required to maintain POMC neuronal activity and energy homeostasis

To determine the expression profile of Mcts in both tanycytes and POMC neurons, we performed qPCR analyses in cells isolated by FACS. POMC neurons where collected from *Pomc::Cre*; *tdTomato*$^{loxP\text{-}STOP\text{-}loxP}$ mice (Figure 3A and Figure S2A-S2C) and tanycytes from wild-type mice infused with the AAV1/2 vector expressing GFP under the tanycyte-specific iodothyronine deiodinase 2 (*Dio2*) promoter (27) into the lateral ventricle (Figure 3A and Figure S2D and S2F). Tanycytes were found to be enriched in *Mct1* (unpaired Student's t-test, *P*=0.0009, 5 and 4 mice) and *Mct4* transcripts (unpaired Student's t-test, *P*=0.0272, n=5 and 4 mice), whereas POMC neurons were rich in *Mct2* mRNA (unpaired Student's t-test, *P*=0.0028, 5 and 4 mice) (Figure 3B). To determine the relative physiological roles of these Mcts in the function of POMC neurons, we first blunted the expression of Mct2 in POMC neurons by injecting a Cre-dependent FLEXon viral vector expressing an shRNA to silence *Mct2* into the ARH of *Pomc::Cre* mice. The expression of *Mct2* shRNA specifically in POMC neurons (Figure S3A) led to a clear increase in cumulative food intake (Figures S3B) and a transient trend to increased weight gain (Figure S3C), in keeping with their anorexigenic function and the effect of blocking lactate uptake by these neurons on their activity seen in Figure 2G-2I. Next, we focused on tanycytic Mcts by co-injecting a Cre-dependent FLEXon viral vector expressing shRNAs to silence *Mct1* and *Mct4* and a *Dio2::Cre* vector into the lateral

ventricle of wild-type or *tdTomato*^{POMC} mice to target tanycytes. FACS-isolation of viral-GFP-expressing cells showed that the *Dio2::Cre*-mediated expression of shRNAs targeting *Mct1* and *Mct4* decreased the expression of these gene transcripts 2-fold selectively in tanycytes (ordinary one-way ANOVA followed by Tukey's post hoc test; Mct1, *P*=0.0231; Mct4, *P*=0.0320; n=4 mice) but not in non-tanycytic cells (*Mct1*: *P*=0.8494, *Mct4*: *P*=0.8944, 4 mice) (Figure 3C and 3D). While *Mct1* and *Mct4* knockdown in tanycytes (*Mct1/4*^{tanycyteKD}) had no effect on the expression of tanycytic markers (unpaired Student's t-test; *Vimentin*, *P*=0.2256; *Dio2*, *P*=0.4034; 4 mice) (Figure S4A and S4B) or on other genes related to glucose metabolism or transport in tanycytes (unpaired Student's t-test; *Mct2*, *P*=0.8204; *Ldha*, *P*=0.5561; *Ldhb*, *P*=0.5457; *Gck*, *P*=0.1381; *Glut1*, *P*=0.2479; *Glut4*, *P*=0.9174; *Cx30*, *P*=0.7825; *Cx43*, *P*=0.4315; 6 mice) (Figure S4C), it markedly dampened spontaneous neuronal firing in POMC neurons (Mann-Whitney U test; *P*=0.0026; 26 cells, 5 mice) (Figure 3E-3G).

Interestingly, *Mct1/4*^{tanycyteKD} mice gained significantly more weight than mice injected with the virus expressing scrambled shRNAs (unpaired Student's t-test; *P*=0.0334, n=7 mice per group) (*Mct1/4*^{tanScramble} Figure 3H). However, surprisingly, this weight gain was not associated with increased food intake (two-way ANOVA followed by an uncorrected Fisher's LSD test; dark phase, *P*=0.2454; light phase, *P*=0.8866; mean, *P*=0.360 (bar graph) and *P*=0.2310 (line graph); 6 *Mct1/4*^{TanScramble} mice and 8 *Mct1/4*^{TanycyteKD} mice) (Figure 3I, see also Figure S4D). Furthermore, although these tanycytic *Mct1/4* knockdown mice showed only mild perturbations in energy expenditure (two-way ANOVA followed by an uncorrected Fisher's LSD test; *P*=0.04480, 7 *Mct1/4*^{TanScramble} mice and 8 *Mct1/4*^{TanycyteKD} mice) (Figure S4E), they displayed a notable loss of both the linear correlation between food intake and body weight (Pearson correlation; *Mct1/4*^{TanScramble}, r^2=0.8087, *P*=0.0378; *Mct1/4*^{TanycyteKD}, r^2=0.08139, *P*=0.5351; 7 mice per group) (Figure 3J) and between energy expenditure and body weight in *Mct1/4*^{tanycyteKD} mice (Pearson's correlation; *Mct1/4*^{TanScramble}, r^2=0.7796, *P*=0.0084; *Mct1/4*^{TanycyteKD}, r^2=0.2481, *P*=0.2553; 7 mice per group) (Figure 3K). Together, these results demonstrate that the maintenance of energy balance is impaired by the reduced tanycytic expression of *Mct1* and *Mct4*.

Given the disconnect between body weight and both food intake and energy expenditure observed above, we further attempted to analyze their respective components to understand the contribution of tanycytic Mcts. An analysis of ambulatory activity showed that while horizontal displacement in the cage appeared to be unchanged between *Mct1/4*^{tanycyteKD} and *Mct1/4*^{tanScramble} mice (two-way ANOVA followed by an uncorrected Fisher's LSD test; *P*=0.5215, 7 *Mct1/4*^{TanScramble} mice and 8 *Mct1/4*^{TanycyteKD} mice)

(Figure S4F), Z-rearing was significantly diminished in *Mct1/4*^{tanycyteKD} mice during the dark phase (two-way ANOVA followed by an uncorrected Fisher's LSD test; dark phase, *P*=0.0012; light phase, *P*=0.3476; mean, *P*=0.0324 (bar graph) and *P*=0.0305 (line graph); 7 *Mct1/4*^{TanScramble} mice and 8 *Mct1/4*^{TanycyteKD} mice) (Figure 3L, see also Figure S4G). This suggests that feeding patterns may differ between these two experimental groups despite similar cumulative food intake (Figure 3I; Figure S4D). Indeed, an analysis of feeding patterns showed that *Mct1/4*^{tanycyteKD} mice ate less frequently than *Mct1/4*^{tanScramble} mice (two-way ANOVA followed by an uncorrected Fisher's LSD test; dark phase, *P*=0.0459; light phase, *P*=0.3042; mean, *P*=0.0037; 5 *Mct1/4*^{TanScramble} mice and 7 *Mct1/4*^{TanycyteKD} mice) (Figure 3M), but that the size of their meals was significantly increased (two-way ANOVA followed by an uncorrected Fisher's LSD test; dark phase, *P*=0.0337; light phase, *P*=0.5919; mean, *P*=0.1018; 5 *Mct1/4*^{TanScramble} mice and 7 *Mct1/4*^{TanycyteKD} mice) (Figure 3N).

Altogether these data suggest that tanycytic lactate shuttles control the activity of POMC neurons and hence contribute to the adaptation of the feeding pattern of the individual to energy needs, i.e., glucose availability.

POMC neuronal activity depends on gap-junction mediated tanycytic metabolic networks

Intriguingly, in the paired tanycyte-neuron recording set-up illustrated in Figure 2E, Lucifer yellow filling the patch pipette diffused from the patched tanycyte into neighboring tanycytes along the wall of the third ventricle. This phenomenon, which was also seen when using biocytin-filled patch pipettes (Figure S5A and S5B), suggests the existence of a functional tanycytic network in the ARH, similar to the gap-junction-mediated astrocytic networks previously described in the brain (28), including in the lateral hypothalamic area (24). The intercellular diffusion of biocytin was blunted by the bath application of the gap-junction blocker, carbenoxolone (CBX; 50 μM; Figure S5C and S5D) (28), suggesting that tanycytes are also connected by gap junctions. Under control conditions, biocytin diffused through the cell bodies of ARH tanycytes over 100-200 μm along the wall of the third ventricle and into tanycytic processes extending into the tissue, but not into cells expressing the neuronal marker NeuN (Figure S5B). In the presence of CBX (50 μM, 30 min), recorded POMC neurons showed a marked decrease in their firing activity (Wilcoxon matched-pair test, *P*=0.0312, 6 cells, 4 mice) (Figure 4A-4C), an effect that could be prevented by the bath application of exogenous lactate (Wilcoxon matched-pair test, *P*=0.625, 5 cells, 4 mice) (Figure 4D and 4E). Interestingly, the treatment of cultured tanycytes with CBX phenocopied

the effects of 4-CIN, i.e. it also prevented the release of lactate into the conditioned medium (one-way repeated measures ANOVA followed by Tukey's post hoc test, *P*=0.0355, n=6) (Figure 2C) and led to its accumulation in the cytoplasm of tanycytes (Figure 2D) (one-way repeated measures ANOVA followed by Tukey's post hoc test, *P*=0.0009, n=6). Together, these results demonstrate functional gap-junctional coupling between tanycytes surrounding POMC neurons in the ARH, and raise the possibility that such glial metabolic networks play a role in the regulation of POMC neuronal activity that is greater than the sum of the roles of individual tanycytes.

In agreement with previous works (29, 30), we found that tanycytes expressed the gap-junction protein connexin-43 (Cx43), with a marked enrichment in ARH tanycytes when compared to median eminence (ME) tanycytes, which are responsible for the transport of glucose and other peripheral metabolic signals into the CSF (22, 25, 31) (Figure S5E-S5G). To determine the functional role of these Cx43-mediated tanycytic networks in the control of the activity of POMC neurons, we next selectively knocked out the *Gja1* gene encoding Cx43 in tanycytes by infusing the recombinant TAT-Cre protein into the third ventricle of *Cx43*$^{loxP/loxP}$ mice (Figure 4F), a procedure that we have extensively characterized before (4, 32). FACS isolation of TAT-Cre-injected *Cx43*$^{+/+}$;*tdTomato*$^{loxP\text{-}STOP\text{-}loxP}$ (*Cx43*$^{+/+}$;*tdTomato*^{Tanycyte}) and *Cx43*$^{loxP/loxP}$;*tdTomato*$^{loxp\text{-}STOP\text{-}loxP}$ (*Cx43*^{TanycyteKO};*tdTomato*^{Tanycyte}) mice (Figure S6), demonstrated that *Cx43* expression is significantly diminished in Tomato-positive tanycytes (unpaired Student's t-test, *P*=0.0449, 6 mice) (Figure 4G), but not in Tomato-negative cells (unpaired Student's t-test, *P*=0.8611, 6 mice) (Figure 4G), which comprise astrocytes that are also known to abundantly express Cx43 (24), in floxed *Cx43* mice. In line with our recent data showing that our TAT-Cre infusion procedure causes genetic recombination in about 60% of ME/ARH tanycytes (33), Cx43 protein expression was fully extinguished in the subset of tanycytes expressing high levels of Tomato (Figure S5I). This submaximal invalidation of Cx43 protein expression in tanycytes was sufficient to abolish the gap-junction mediated tanycytic network, as shown by the absence of intercellular diffusion following biocytin injection into a single ARH tanycyte via a patch pipette (Mann-Whitney U test, *P*=0.0006, 7 and 7 cells, 6 and 6 mice) (Figure S5J and S5K). Consequently, it markedly diminished the ability of energy metabolites to be trafficked between ARH tanycytes, as shown by the injection of a single tanycyte with the fluorescent glucose derivate 2-[N-(7-nitrobenz-2-oxa-1,3-diazol-4-yl)amino]-2-deoxyglucose (2-NBDG; 2 mg/ml) (28) (Figure 4H and 4I) (unpaired Student's t-test, *P*=0.0011, n=5 and 10 cells, 2 and 4 mice). This deletion of Cx43 specifically in tanycytes also decreased spontaneous POMC neuronal firing (Mann-

Whitney U test, *P*=0.0043, 6 and 5 cells, 5 and 4 mice) (Figure 4J-4L), which was restored by the bath application of 5 mM lactate in the presence of 2.5 mM glucose (Wilcoxon matched-pair test, *P*=0.0312, 6 cells, 5 mice) (Figure 4M and 4N). However, in *Cx43*$^{loxP/loxP}$ littermates, the bath application of lactate had no effect on POMC neuronal activity, which was normal (paired Student's t-test, *P*=0.6042, 6 cells, 6 mice) (Figure S5L and S5M). These results suggest that the decreased activity of POMC neurons in *Cx43*^{TanycyteKO} mice results from a deficiency in the trafficking of glucose-derived lactate through the tanycytic network.

Tanycytic *Cx43* knockout impairs changes in ARH lactate levels in response to blood glucose variation

CSF glucose, whose levels are maintained at approximately 60% of serum glucose levels (11, 12), has long been proposed to complete a feedback loop in the homeostatic control of food intake and body weight (34). Regardless of its source, this role of glucose in energy homeostasis appears to require the production of lactate by glial cells in the hypothalamus (17), and central lactate metabolism has been shown to regulate food intake (35, 36). We thus next assessed the putative involvement of gap-junction-mediated tanycytic metabolic networks, which metabolize glucose into lactate (Figure 2C, 2D, 2K-2M), in controlling the bioavailability of lactate in hypothalamic tissue in a physiological context. Microdialysis experiments in the ARH of *Cx43*$^{loxP/loxP}$ mice and littermates in which *Cx43* was knocked out (*Cx43*^{TanycyteKO}) using either the TAT-Cre recombinant protein or the *Dio2::Cre* viral approach (see Figure 5C, right panel for a comparison of the two methods), before and after the intraperitoneal injection of saline and glucose (2g/kg body weight) (Figure 5A-5C) showed that while saline injection did not alter lactate levels (two-way repeated measures ANOVA followed by an uncorrected Fisher's LSD test, 6 and 10 mice; vehicle $_{(40\ min)}$ vs. basal, *P*=0.6663 in *Cx43*$^{loxP/loxP}$ mice and *P*=0.3059 *Cx43*^{TanycyteKO} mice), glucose injection quickly promoted an increase in the hypothalamic levels of lactate in *Cx43*$^{loxP/loxP}$ mice (vehicle $_{(20\ min)}$ vs. glucose $_{(20\ min)}$, *P* = 0.0008 and vehicle $_{(40\ min)}$ vs. glucose $_{(40\ min)}$, *P*<0.0001). In contrast, peripheral glucose injection was found to have no effect on hypothalamic levels of lactate in *Cx43*^{TanycyteKO} mice (vehicle $_{(20\ min)}$ vs. glucose $_{(20\ min)}$, *P* = 0.1153 and vehicle $_{(40\ min)}$ vs. glucose $_{(40\ min)}$, *P*=0.0049), which remained lower than in *Cx43*$^{loxP/loxP}$ animals after glucose injection (*P*=0.0012) at 40 min). Our results suggest that tanycytic metabolic networks along the wall of the third ventricle that are in contact with both the blood circulation and the CSF are actively involved in integrating changes in

circulating glucose levels and translating these changes into a local lactate signal that can be perceived by ARH neurons and used to drive their activity. Furthermore, downregulation of the expression of the glucose transporter *Glut2* (unpaired Student's t-test, *P*=0.0071, 6 mice) and lactate dehydrogenase *Ldhb* (unpaired Student's t-test, *P*=0.0119, 6 mice) in tanycytes knocked out for *Cx43* (Figure 5D) may further accentuate the shortage of tanycytic lactate supply to ARH neurons in mutant mice.

Knockout of *Cx43* in ARH tanycytes causes weight gain and modulates substrate consumption

Supporting the role of the glucose-sensitive tanycytic network in modulating the activity of POMC neurons controlling food intake in response to the peripheral energy state, $Cx43^{TanycyteKO}$ mice showed increased food intake (unpaired Student's t-test, *P*=0.0428, 7 and 9 mice) (Figure 5E), body weight (unpaired Student's t-test, *P*=0.0121, 9 mice per group) (Figure 5F) and fat mass content (unpaired Student's t-test, *P*=0.0287, 8 and 9 mice) (Figure 5G), but no change in lean mass (Mann-Whitney U test, *P*=0.1139, 8 and 9 mice) (Figure 5H), when compared to vehicle-injected $Cx43^{loxP/loxP}$ littermates 10 days after Tat-cre injection into the third ventricle. Given that the central melanocortin system not only modulates feeding but also controls energy partitioning and expenditure (37-40), we further investigated the role of tanycytic Cx43 in the regulation of energy homeostasis. $Cx43^{loxP/loxP}$ mice were subjected to indirect calorimetry before and after TAT-Cre injection. After TAT-Cre injection, $Cx43^{TanycyteKO}$ mice, in addition to the increase in food intake noted above (two-way ANOVA, uncorrected Fisher's LSD test, *P*=0.0001, 7 mice per group) (Figure 5I), showed a decrease in ambulatory activity (two-way ANOVA, uncorrected Fisher's LSD test, *P*<0.0001, 7 mice per group) (Figure 5J) and in energy expenditure (two-way ANOVA, uncorrected Fisher's LSD test, *P*=0.0001, 7 mice per group) (Figure 5K). Importantly, selectively knocking out Cx43 in tanycytes also induced a marked increase in the respiratory exchange ratio (two-way ANOVA, uncorrected Fisher's LSD test, *P*=0.0147, 7 mice per group) (Figure 5L) together with a decrease in oxygen consumption (Figure 5M), both during the resting phase (day; unpaired Student's t-test, *P*=0.0394, 7 mice per group) and during the active phase (night; unpaired Student's t-test *P*=0.0261, 7 mice per group). The higher respiratory exchange ratio in $Cx43^{TanycyteKO}$ mice suggests that nutrient partitioning is altered, favoring the use of carbohydrates (CHO) rather than fatty acids (FA) as an energy source in these mice, contrary to the normal situation (41). In addition to dramatically impairing POMC neuronal activity (Figure 4K and 4L), these changes in metabolism after the selective knockout of *Cx43* in tanycytes were associated with an upregulation of transcripts for NPY

in the ARH (unpaired Student's t-test, *P*=0.0492, 6 mice) while transcripts for POMC (unpaired Student's t-test, *P*=0.6335, 6 mice), CART (unpaired Student's t-test, *P*=0.4184, 6 mice) and AgRP (unpaired Student's t-test, *P*=0.4722, 6 mice) appeared to be unchanged in mutant mice (Figure 5N). The gap-junction-mediated ARH tanycytic network thus appears to be a physiologically relevant component of metabolic regulation, modulating feeding behavior and the establishment of energy balance in response to peripheral conditions.

DISCUSSION

The question of what energy metabolites reach POMC neurons in the ARH has a twofold significance: first, like every other type of neuron, POMC neurons need an energy source to drive their activity; but second and more importantly, the activity of these anorexigenic neurons is itself to control the energy state of the organism, making it essential for them to sense metabolic signals triggered by nutrient intake or energy consumption at the periphery.

Our results shed new light on a long-established but ill-understood phenomenon (10, 42, 43) by demonstrating that POMC neurons depend on the bioavailability of lactate for their activity, and that this lactate is metabolized from glucose and distributed to neurons by a network of ARH tanycytes. Intriguingly, the dramatic suppression of POMC neuronal activity in mice in which lactate transfer by tanycytes is blocked indicates that with regard to this neuronal population at least, the astrocyte-neuron lactate shuttle (23, 44), which up to now was thought to explain the regulation of synaptic transmission and the fueling of neuronal activity in neocortical (28) and hypothalamic brain regions (24), has been almost completely replaced by a shuttle consisting of another glial cell type, the tanycytes. This places tanycytes at the center of the intercellular communication processes used by hypothalamic circuits regulating energy homeostasis, where they play the role of bloodhounds of the metabolic brain, "sniffing" out the availability of glucose and conveying this information to neurons in such a way as to modulate their activity. Indeed, studies in human patients lacking the glucose transporter GLUT1 suggest that CSF-borne peripheral glucose is an important source of lactate in the brain (45). The peculiar position occupied by tanycytes, at the interface of both the peripheral circulation and the CSF, makes them ideal candidates for the detection and perhaps the triangulation of circulating metabolic signals, potentially providing qualitative in addition to quantitative information. Importantly, the fact that the energy metabolite released by ARH tanycytes and used by POMC neurons to adjust their activity to

physiological demands is lactate and not glucose provides a plausible explanation for why POMC neurons, whose function it is to respond to changes in glucose levels, do not themselves appear to be capable of sensing glucose (9). Furthermore, consistent with the notion that non-neuronal cells are functionally involved in the regulation of metabolic sensing and the central control of systemic metabolism (33, 46-48), recent studies have reported that insulin receptor expression in astrocytes is involved in the regulation of glucose uptake at the blood-brain barrier (46) and may participate in the glucose-induced activation of POMC neurons, possibly via changes in the glial coverage of POMC neuronal cell bodies (46, 49). It remains to be determined whether and how this newly uncovered role for astrocytes modulates the role of tanycytes, or vice versa, in the fine-tuning of POMC neuronal function.

Intriguingly, our findings reveal both the involvement of the monocarboxylate transporters Mct1 and Mct4 and a previously unknown role for Cx43 gap-junction channels in the transfer of lactate to POMC neurons by ARH tanycytes. Indeed, the connexins appear to constitute the molecular basis of the newly discovered metabolic network formed by these CSF-contacting tanycytes. The ability to mobilize and transfer lactate through a large number of interconnected cells may serve to increase the sensitivity of the response to any peripheral signal beyond the sum of the responses of a number of unconnected cells, each releasing its own load of lactate. In addition to this amplification of the efficiency with which a metabolic signal reaches its targets, the existence of these gap-junction-mediated tanycytic networks could improve the adaptive metabolic response by synchronizing the release of energy metabolites to neuronal populations that need to be informed about variations in physiological state.

Keeping in mind the fact that blocking or knocking out Cx43 specifically in ARH tanycytes phenocopies the effect of the Mct inhibitor 4-CIN, the potential involvement of connexin hemichannels themselves in the secretion of lactate by tanycytes (50), or a signaling role for gap junctions above and beyond the transfer of metabolites between tanycytes, cannot be ruled out. A putative signaling role for Cx43 in the control of tanycytic lactate secretion is suggested by our *in vitro* data showing that treatment of cultured tanycytes with the gap junction blocker carbenoxolone alters lactate release (Figure 2C). Strengthening this possibility are also our *in vivo* results showing that knocking out *Cx43* in tanycytes results in the downregulation of two critical molecules specifically in these cells: the glucose transporter *Glut2*, which has recently been suggested to promote the rapid transfer of circulating glucose into the CSF at the median eminence (31), and the lactate dehydrogenase *Ldhb*. Together with the recent demonstration

that Cx43 can directly act as a transcriptional regulator (51), these results raise the intriguing possibility that *Cx43* may form a functional micronetwork with other genes, e.g. *Glut2* and *Ldhb,* in tanycytes, although it remains to be determined whether such a micronetwork would simply dictate the terms of glucose conversion into lactate, or would itself be subject to feedback regulation by accumulating intracellular lactate that has nowhere to go when Cx43 or the Mcts are blocked.

The physiological relevance of these results is demonstrated by the phenotype of mice lacking Cx43 in ARH tanycytes. Their inability to metabolize lactate from glucose and the resulting lower activity of POMC neurons cause a profound metabolic dysfunction represented by hyperphagia, increased weight gain and adiposity, decreased energy expenditure and an increased respiratory exchange ratio, indicating a switch from lipid to carbohydrate use. It is well established that the central melanocortin system, of which the POMC neurons form an integral element, regulates all these parameters. Interestingly, our mice in which tanycytic Cx43 is inactivated appear to phenocopy those lacking POMC (52, 53) or melanocortin receptor 4 (54). This, together with the fact that the selective impairment of Mct1 and Mct4 expression in tanycytes is as effective at inhibiting POMC neuronal activity as knocking out Cx43 in these cells, strongly suggests that the low bioavailability of tanycytic lactate shuts down the activity of POMC neurons, and that this deficiency cannot be compensated by any other neuroglial pathway. Strengthening this idea are our patch-clamp experiments showing that the direct infusion of the lactate dehydrogenase inhibitor oxamate into the Cx43-connected tanycytic network, effectively abolishing the conversion of bath-borne glucose into lactate by tanycytes, suffices to blunt the spontaneous firing of POMC neurons in living brain slices. In addition, the selective knockdown of the expression of Mct1 and Mct4 in tanycytes also provides a more nuanced view of the manner in which these cells influence food intake. Indeed, the lack of tanycytic Mct1/4 not only dramatically impairs the spontaneous activity of POMC neurons, but the resulting body weight gain occurs without a marked change in cumulative food intake, instead altering meal patterns and uncoupling both energy intake and energy expenses from bodily needs, unlike the more straightforward effect observed when *Mct2* alone was knocked down in POMC neurons. These results agree with previous studies showing that the activity of a subpopulation of ARH POMC neurons projecting to the brainstem controls feeding behavior, and that the inhibition of melanocortinergic activity in the brainstem nucleus of the solitary tract increases meal size (55, 56). Another interesting question, however, is whether the tanycytic lactate shuttle or gap-junctional network is required for the activity of other hypothalamic neurons, such as the orexigenic

AgRP/NPY neurons, which play an opposite role to that of POMC neurons in energy homeostasis (6, 9) but which are also rich in Mct2 and may play a confounding role when *Mct2* is silenced in POMC neurons (57). Our results indeed show that knocking out Cx43 in tanycytes upregulates NPY transcripts in the mediobasal hypothalamus. Whether this change, which may, at least in part, contribute to the increased feeding in mutant mice, is a direct or an indirect consequence of the impaired tanycytic lactate shuttle remains to be explored.

In conclusion, our results reveal an unexpected role for tanycytic networks connected by gap junctions, thanks to their unique position and ability to convert glucose into lactate, as both the suppliers of energy metabolites to fuel the activity of hypothalamic POMC neurons that regulate energy homeostasis, and as the sensors of peripheral energy state upstream of these neurons. Further investigation into how tanycytes, which bridge the blood and CSF, perceive and translate this information for neurons could clear the way to potential treatments for metabolic disorders such as obesity and type 2 diabetes.

METHODS

Animals

The experiments used wild-type C57Bl/6J and single, double or triple transgenic *Cx43*$^{loxP/loxP}$ (RRID_JAX008039), *Pomc*::*Cre* (RRID:IMSR_JAX:005965) and *tdTomato*$^{loxP\text{-}STOP\text{-}loxP}$ (RRID:IMSR_JAX007914) and *Cx43*$^{loxP/loxP}$;*tdTomato*^{POMC} mice maintained on a C57Bl6 background as detailed in the Supplementary Methods. All mice were bred and housed in a temperature- and humidity-controlled room on a 12h/12h light/dark cycle and with access to food and water ad libitum.

Stereotaxic delivery of viruses to manipulate the expression of Mcts in POMC neurons and tanycytes

In POMC neurons. AAV8[FLEXon]-SYN1 (EGFP:miR30_MCT-2[mSlc16a7]) (1.17 x 1013 PFU/ml, Vector Builder, Vector ID: VB200715-1173hzs) and AAV-GFP scrambled (1.1 x 1013 PFU/ml, Vector Builder) were injected into the ARH of POMC-Cre mice (58, 59). The ARH was targeted bilaterally and AAVs were delivered at a rate of 0.1 µl/min for 5 min (0,5 µl/injection site) according to the following coordinates: -1.5 mm posterior to the bregma, ± 0.2 mm lateral to midline, and -6 mm below the surface of the skull. Specific transduction of POMC neurons by AAVs was evaluated by immunohistochemistry. Body weight and food intake were recorded over 5 weeks after the surgery.

In tanycytes. Wild-type C57Bl/6J or *tdTomato*^{POMC} mice were injected either with 2μl of a 1/1 mix of AAV1/2[FLEXon]-CMV (EGFP:miR30_shRNA-MCT-1[mSlc16a1]_shRNA-MCT-4[mSlc16a3]) (at a titer of 4.4x10^9 gp/μl; VectorBuilder, Vector ID: VB200716-1259yky) and AAV1/2-Dio2:Cre (at a titer of 2.2x10^10 gp/μl) (27) (n=4) or 2μl of a 1/1 mix of AAV1/2[FLEXon]-CMV (EGFP:miR30_scramble) (at a titer of 1.6x10^10 gp/μl) and AAV1/2-Dio2:Cre (at a titer of 2.2x10^10 gp/μl) (n=4) at a rate of 0.3μl/min. All animals were injected into the lateral ventricle (coordinates from bregma AP: -0.3mm, ML: -1mm and DV: -2.5mm from skull).

Stereotaxic TAT-Cre delivery

Tanycyte-specific Cx43 deletion was performed using the Cre/LoxP system by stereotaxically infusing a TAT-Cre fusion protein into the third ventricle (2 μl; 0.3 μl/min; anteroposterior/midline/ dorsoventral coordinates: -1.7 mm / 0 mm / -5.6 mm) in isoflurane-anesthetized Cx43$^{loxP/loxP}$ mice or Cx43$^{loxP/loxP}$;tdTomato^{POMC} mice one week before experiments. The TAT-Cre fusion protein was produced as detailed previously (4). For control mice, a vehicle solution was injected.

Brain slice preparation

Electrophysiological recordings were performed on living brain slices containing the tuberal region of the hypothalamus from 8- to 12-week-old mice as previously described (59). Briefly, mice were anesthetized with isoflurane and decapitated. The brain was removed and rapidly placed in ice-cold artificial cerebrospinal fluid (ACSF) containing the following (in mM): 120 NaCl, 3.2 KCl, 1 NaH_2PO_4, 26 $NaHCO_3$, 1 $MgCl_2$, 2 $CaCl_2$, 2.5 glucose (290 mOsm, pH 7.4) and bubbled with 95% O_2-5% CO_2. Three 250 μm-thick coronal hypothalamic slices containing the arcuate nucleus were cut using a vibratome (VT1200; Leica). Slices were incubated at 34°C in oxygenated ACSF for a recovery period of 1 hour, and then at room temperature until recording.

Patch-clamp recording

For patch-clamp recording, individual brain slices were placed in a submerged recording chamber (Warner Instruments), immobilized by a nylon grid and continuously perfused at a rate of 3 ml/min with oxygenated ACSF maintained at 32.8°C by a heater controller (TC-344C; Warner Instruments). POMC neurons and ARH tanycytes were visualized and identified under 40x magnification using an upright

fluorescent microscope with infrared differential interference contrast (Leica DM-LFSA) and an ORCA-Flash4.0 digital CMOS camera (Hamamatsu). Recording pipettes were pulled from borosilicate glass capillaries (1.5 mm outer diameter; 1.12mm inner diameter; World Precision Instruments) using P1000 Flaming Brown puller (Sutter Instruments Co) and had a resistance of 4 to 6 MΩ when filled with an internal solution containing the following (in mM): 123 K-gluconate, 2 $MgCl_2$, 8 KCl, 0.2 EGTA, 4 Na_2-ATP, 0.3 Na-GTP, and 10 HEPES, pH 7.3 with KOH. In paired recordings of a tanycyte and a neuron, sodium L-lactate (5 mM; Alfa Aesar, Cat#L14500, CAS:867-56-1) was also added to the internal solution of the tanycyte pipette. Pipettes were placed in contact with a POMC neurons or an ARH tanycyte using a PCS-5400 micromanipulator (Thorlabs). Whole-cell patch-clamp recordings were performed in current-clamp mode using a Multiclamp 700B Amplifier, digitized with the Digidata 1322A interface and acquired with pClamp 10.2 software (Molecular Devices). Data were filtered at 1 kHz and sampled at 5 kHz.

For exogenous glucose deprivation studies, the osmolarity of the ACSF containing 0 mM D-glucose was adjusted with sucrose. All drugs tested (Alpha-cyano-4-hydroxycinnamate (4-CIN), 500 μM, Sigma, Cat#C2020, CAS:28166-41-8; sodium oxamate, 10 mM, Sigma, Cat#O2751, CAS 565-73-1; sodium L-lactate, 5 mM, Alfa Aesar; sodium pyruvate, 5 mM, Sigma, Cat#P2256, CAS:113-24-6; carbenoxolone disodium salt (CBX), 50 μM, Sigma, Cat#C4790, CAS:7421-40-1) were applied to the perfusion system after stable baseline recording.

Recordings were analyzed with Clampfit 10.2 from pClamp software (Molecular Devices). For each recording, membrane potential and mean firing rate were determined before and during the bath application of drugs. Neurons were considered responsive when a change of more than 20% in firing rate was observed. The peak response was determined, and the number of spikes was counted 3 min before and after the peak effect.

For glucose and dye diffusion experiments, the internal solution contained the fluorescent glucose derivate 2-[N-(7-notrobenz-2-oxa-1,3-diazol-4-y)amino]-2-desoxyglucose (2-NBDG, 2mg/ml, Invitrogen, Cat#N13195, CAS:186689-07-6) or biocytin (2mg/ml, Sigma, Cat#B4261, CAS: 576-19-2), respectively. Recorded cells were loaded with these solutions for 20 minutes in current-clamp mode. The intercellular diffusion of 2-NBDG was captured online with a digital camera just after recording and diffusion distance was analyzed with Fiji software. Biocytin diffusion was revealed by Alexa Fluor 488 streptavidin (Invitrogen Cat#S11223) as detailed in the Supplementary Methods and analyzed using an Axio Imager

Z2 Apotome microscope (AxioCam 504 MRm camera, Zeiss). To inhibit gap-junctional communication, slices were pretreated for 20 minutes with 50 µM CBX.

For dye diffusion during paired tanycyte-neuron recordings, one ARH tanycyte was recorded and filled with the gap-junction permeable Lucifer yellow CH dilithium salt (1 mg/ml; Sigma, Cat#L0259, CAS:67769-47-5) through the patch pipettes; one neighboring POMC neuron was then similarly recorded and filled with the membrane-impermeable dye Alexa Fluor 594 hydrazide (40 mM; Invitrogen, Cat#A10438). Images were captured 20 minutes after recording using a digital camera.

Primary cultures of tanycytes

Primary cultures of tanycytes were generated by isolating the median eminence of 10-day-old Sprague-Dawley rats (Janvier Laboratories, Saint Berthevin, France), as described previously (26), and processed as described in the Supplementary Methods.

Fluorescence-activated cell sorting (FACS) and qPCR

FACS isolation of hypothalamic neurons and tanycytes and subsequent qPCR analyses were performed according to the previously described protocols (33, 60), with some adaptations, as detailed in the supplementary methods.

Immunochemistry

Immunocytofluorescence protocols are detailed in the Supplementary Methods. Primary antibodies were anti-Cx43 (Millipore Cat#AB1727, RRID:AB_2294609, 1:200), anti-MCT-1 (Millipore Cat#AB1286, RRID:AB_11212410, 1:100), anti-MCT-4 (Millipore, 1:200), anti-Vimentin (Millipore Cat#AB3314P, RRID:AB_2286063, 1:1000 and DAKO Cat#M0725, RRID:AB_10013485, 1:100), anti-NeuN (1:1000; Millipore, Cat#MAB377, RRID:AB_2298772), anti-POMC propeptide (1:200; Phoenix pharmaceuticals, Cat#H02930, RRID:AB_2307442), and anti-GFP (1:1000; Invitrogen, Cat#A10262, RRID:AB_2534023). Immunofluorescence images were captured using an Axio Imager Z2 Apotome microscope or an LSM 710 Zeiss confocal microscope.

Metabolic studies

Analysis of basal metabolism. Mice were analyzed for total energy expenditure, oxygen consumption and carbon dioxide production, food intake and ambulatory movements (total beam breaks/h) using calorimetric cages (TSE Systems GmbH, Germany) and standard procedures published by others (61, 62). Mice were individually housed and acclimatized to the cages for 48h before experimental measurements.

Body weight and composition. Fat and lean tissue mass were determined by Nuclear Magnetic Resonance (MiniSpec mq 7.5, RMN Analyser, Bruker) according to the manufacturer's recommendations.

In vivo brain microdialysis

Male $Cx43^{loxP/loxP}$ and $Cx43^{tanKO}$ mice of 30-35g were deeply anesthetized with isoflurane (3% in 1 l/min air flow) in an induction chamber, and placed in a stereotaxic apparatus equipped with a mask to maintain anesthesia throughout the experiment (isoflurane 1% in 0.7 l/min air flow). Core body temperature was maintained at 37°C with an electrical blanket controlled by a thermostat. A microdialysis cannula (CMA7, 6 kDa, 2 mm membrane length; CMA microdialysis AB, Sweden) was implanted over the hypothalamic area using stereotaxic coordinates (anteroposterior: -1.4, lateral: −0.3, ventral: −6.0 mm relative to bregma). The microdialysis probe was then perfused with sterile ACSF (CMA Perfusion Fluid CNS, in mM: 147 NaCl, 2.7 KCl, 1.2 CaCl2 and 0.85 MgCl2; CMA, Stockholm, Sweden) at a rate of 2 µl/min using a microinjection pump (CMA 402; CMA, Stockholm, Sweden). Following a stabilization period of 60 min (two dialysates of 10 min each were collected at 40 and 50 min), a sterile vehicle injection (i.p., 0.9% NaCl) was administered to the mice and four dialysates of 10 min each were recovered. At 100 min, a glucose solution was administered to the mice (i.p., 2g/kg in saline) and seven dialysates of 10 min each were recovered. Brain dialysates were placed in a fraction collector (CMA/820) during the experiment and immediately stored at −80°C until analysis. At the end of the experiment, mice were euthanized by decapitation and brains stored immediately in fresh 4% paraformaldehyde. The lactate content of microdialysates from the brain was measured using a luminometric Lactate-Glo™ assay kit (Promega), according to the manufacturer's protocol, using a Varioskan LUX microplate reader (Thermo Scientific Inc.).

Statistics

Data are presented as means ± standard errors of the mean (S.E.M). All statistical analyses were performed using GraphPad Prism Software Version 7 (GraphPad, San Diego, CA) and are reported in Table S1. To compare two groups, an unpaired two-tailed Student's t-test or paired Student's t-test was used for normal distributions and a Wilcoxon matched-pair test or a Mann-Whitney U test was performed for non-Gaussian distributions. To compare several groups, a one-way ANOVA followed by Tukey's post hoc multiple comparison test or a two-way ANOVA followed by an uncorrected Fisher's LSD test was used. Repeated-measures ANOVAs were used when multiple measurements were made over time in the same groups. P values < 0.05 were considered statistically significant.

Study approval

Ethical approval for animal studies was obtained from the French Ministry of National Education, Higher Education and Research (APAFIS#2617-2015110517317420 v5 and APAFIS#13387-2017122712209790 v9) in France and by the Ethics Committee of the University of Santiago de Compostela, in accordance with European Union norms for experimental animals.

ACKNOWLEDGMENTS

This work was supported by the European Research Council (ERC) Synergy Grant WATCH no. 810331 to R. N., V.P. and M.S., the H2020-MSCA-IF-2014, ID656657 to J.C. and the H2020-MSCA-IF-2016, ID748134 to M.I. and the Region Hauts-de-France VisionAIRR grant n°189090. We thank Meryem Tardivel (Confocal microscopy) and Nathalie Jouy (Flow cytometry) from the BioImaging Center of Lille (BiCeL), and Julien Devassine (animal core facility) of the UMS2014-US41 for their expert technical support.

AUTHORS CONTRIBUTIONS

T.L. and J.C. carried out the electrophysiological and neuroanatomical experiments. F.S. performed the experiments in primary cultures. J.C., E.C. and M.I. conducted the metabolic phenotyping of the mice. D.F., M.I. and I.M.-C. performed the microdialysis experiments and T.L., M.I., D.F., N.S.L, V.H.D., and H.M.F. experiments involving AAVs. T.L., J.C., M.I., D.F., S.R., M.S., R.N., and V.P. designed and planned the study. All authors contributed to the preparation of the manuscript.

REFERENCES

1. De Vivo DC, Trifiletti RR, Jacobson RI, Ronen GM, Behmand RA, and Harik SI. Defective glucose transport across the blood-brain barrier as a cause of persistent hypoglycorrhachia, seizures, and developmental delay. *N Engl J Med.* 1991;325(10):703-9.
2. Wang D, Pascual JM, Yang H, Engelstad K, Mao X, Cheng J, et al. A mouse model for Glut-1 haploinsufficiency. *Hum Mol Genet.* 2006;15(7):1169-79.
3. Fox PT, Raichle ME, Mintun MA, and Dence C. Nonoxidative glucose consumption during focal physiologic neural activity. *Science.* 1988;241(4864):462-4.
4. Langlet F, Levin BE, Luquet S, Mazzone M, Messina A, Dunn-Meynell AA, et al. Tanycytic VEGF-A Boosts Blood-Hypothalamus Barrier Plasticity and Access of Metabolic Signals to the Arcuate Nucleus in Response to Fasting. *Cell Metab.* 2013;17(4):607-17.
5. Dunn-Meynell AA, Sanders NM, Compton D, Becker TC, Eiki J, Zhang BB, et al. Relationship among brain and blood glucose levels and spontaneous and glucoprivic feeding. *J Neurosci.* 2009;29(21):7015-22.
6. Claret M, Smith MA, Batterham RL, Selman C, Choudhury AI, Fryer LG, et al. AMPK is essential for energy homeostasis regulation and glucose sensing by POMC and AgRP neurons. *J Clin Invest.* 2007;117(8):2325-36.
7. Parton LE, Ye CP, Coppari R, Enriori PJ, Choi B, Zhang CY, et al. Glucose sensing by POMC neurons regulates glucose homeostasis and is impaired in obesity. *Nature.* 2007;449(7159):228-32.
8. Levin BE, Routh VH, Kang L, Sanders NM, and Dunn-Meynell AA. Neuronal glucosensing: what do we know after 50 years? *Diabetes.* 2004;53(10):2521-8.
9. Fioramonti X, Contie S, Song Z, Routh VH, Lorsignol A, and Penicaud L. Characterization of glucosensing neuron subpopulations in the arcuate nucleus: integration in neuropeptide Y and pro-opio melanocortin networks? *Diabetes.* 2007;56(5):1219-27.
10. Levin BE. Neuronal glucose sensing: still a physiological orphan? *Cell Metab.* 2007;6(4):252-4.
11. Fishman RA. Carrier Transport of Glucose between Blood and Cerebrospinal Fluid. *Am J Physiol.* 1964;206:836-44.
12. Nigrovic LE, Kimia AA, Shah SS, and Neuman MI. Relationship between cerebrospinal fluid glucose and serum glucose. *N Engl J Med.* 2012;366(6):576-8.
13. Magistretti PJ, and Allaman I. Lactate in the brain: from metabolic end-product to signalling molecule. *Nat Rev Neurosci.* 2018;19(4):235-49.
14. Prevot V, Dehouck B, Sharif A, Ciofi P, Giacobini P, and Clasadonte J. The Versatile Tanycyte: A Hypothalamic Integrator of Reproduction and Energy Metabolism. *Endocr Rev.* 2018;39(3):333-68.
15. Garcia-Caceres C, Balland E, Prevot V, Luquet S, Woods SC, Koch M, et al. Role of astrocytes, microglia, and tanycytes in brain control of systemic metabolism. *Nat Neurosci.* 2019;22(1):7-14.
16. Parsons MP, and Hirasawa M. ATP-sensitive potassium channel-mediated lactate effect on orexin neurons: implications for brain energetics during arousal. *J Neurosci.* 2010;30(24):8061-70.
17. Lam TK, Gutierrez-Juarez R, Pocai A, and Rossetti L. Regulation of blood glucose by hypothalamic pyruvate metabolism. *Science.* 2005;309(5736):943-7.
18. Sanders NM, Dunn-Meynell AA, and Levin BE. Third ventricular alloxan reversibly impairs glucose counterregulatory responses. *Diabetes.* 2004;53(5):1230-6.
19. Elizondo-Vega R, Cortes-Campos C, Barahona MJ, Oyarce KA, Carril CA, and Garcia-Robles MA. The role of tanycytes in hypothalamic glucosensing. *J Cell Mol Med.* 2015;19(7):1471-82.
20. Frayling C, Britton R, and Dale N. ATP-mediated glucosensing by hypothalamic tanycytes. *J Physiol.* 2011;589(Pt 9):2275-86.
21. Cortes-Campos C, Elizondo R, Llanos P, Uranga RM, Nualart F, and Garcia MA. MCT expression and lactate influx/efflux in tanycytes involved in glia-neuron metabolic interaction. *PLoS One.* 2011;6(1):e16411.
22. Nilaweera K, Herwig A, Bolborea M, Campbell G, Mayer CD, Morgan PJ, et al. Photoperiodic regulation of glycogen metabolism, glycolysis, and glutamine synthesis in tanycytes of the Siberian hamster suggests novel roles of tanycytes in hypothalamic function. *Glia.* 2011;59(11):1695-705.
23. Pellerin L, and Magistretti PJ. Glutamate uptake into astrocytes stimulates aerobic glycolysis: a mechanism coupling neuronal activity to glucose utilization. *Proc Natl Acad Sci U S A.* 1994;91(22):10625-9.

24. Clasadonte J, Scemes E, Wang Z, Boison D, and Haydon PG. Connexin 43-Mediated Astroglial Metabolic Networks Contribute to the Regulation of the Sleep-Wake Cycle. *Neuron.* 2017;95(6):1365-80 e5.
25. Balland E, Dam J, Langlet F, Caron E, Steculorum S, Messina A, et al. Hypothalamic tanycytes are an ERK-gated conduit for leptin into the brain. *Cell Metab.* 2014;19(2):293-301.
26. Prevot V, Cornea A, Mungenast A, Smiley G, and Ojeda SR. Activation of erbB-1 signaling in tanycytes of the median eminence stimulates transforming growth factor beta1 release via prostaglandin E2 production and induces cell plasticity. *JNeurosci.* 2003;23(33):10622-32.
27. Muller-Fielitz H, Stahr M, Bernau M, Richter M, Abele S, Krajka V, et al. Tanycytes control the hormonal output of the hypothalamic-pituitary-thyroid axis. *Nat Commun.* 2017;8(1):484.
28. Rouach N, Koulakoff A, Abudara V, Willecke K, and Giaume C. Astroglial metabolic networks sustain hippocampal synaptic transmission. *Science.* 2008;322(5907):1551-5.
29. Szilvasy-Szabo A, Varga E, Beliczai Z, Lechan RM, and Fekete C. Localization of connexin 43 gap junctions and hemichannels in tanycytes of adult mice. *Brain Res.* 2017;1673:64-71.
30. Recabal A, Elizondo-Vega R, Philippot C, Salgado M, Lopez S, Palma A, et al. Connexin-43 Gap Junctions Are Responsible for the Hypothalamic Tanycyte-Coupled Network. *Front Cell Neurosci.* 2018;12:406.
31. Martinez F, Cifuentes M, Tapia JC, and Nualart F. The median eminence as the hypothalamic area involved in rapid transfer of glucose to the brain: functional and cellular mechanisms. *J Mol Med (Berl).* 2019;97(8):1085-97.
32. Parkash J, Messina A, Langlet F, Cimino I, Loyens A, Mazur D, et al. Semaphorin7A regulates neuroglial plasticity in the adult hypothalamic median eminence. *Nat Commun.* 2015;6:6385.
33. Duquenne M, Flogueira C, Bourouh C, Millet M, Silva A, Clasadonte J, et al. Leptin brain entry via a tanycytic LepR:EGFR shuttle controls lipid metabolism and pancreas function. *Nat Metab.* 2021:in press.
34. Steffens AB, Scheurink AJ, Porte D, Jr., and Woods SC. Penetration of peripheral glucose and insulin into cerebrospinal fluid in rats. *Am J Physiol.* 1988;255(2 Pt 2):R200-4.
35. Lam CK, Chari M, Wang PY, and Lam TK. Central lactate metabolism regulates food intake. *Am J Physiol Endocrinol Metab.* 2008;295(2):E491-6.
36. Cha SH, and Lane MD. Central lactate metabolism suppresses food intake via the hypothalamic AMP kinase/malonyl-CoA signaling pathway. *Biochem Biophys Res Commun.* 2009;386(1):212-6.
37. Lee YS, Challis BG, Thompson DA, Yeo GS, Keogh JM, Madonna ME, et al. A POMC variant implicates beta-melanocyte-stimulating hormone in the control of human energy balance. *Cell Metab.* 2006;3(2):135-40.
38. Denis RG, Joly-Amado A, Cansell C, Castel J, Martinez S, Delbes AS, et al. Central orchestration of peripheral nutrient partitioning and substrate utilization: implications for the metabolic syndrome. *Diabetes Metab.* 2014;40(3):191-7.
39. Krashes MJ, Lowell BB, and Garfield AS. Melanocortin-4 receptor-regulated energy homeostasis. *Nat Neurosci.* 2016;19(2):206-19.
40. Gautron L, Elmquist JK, and Williams KW. Neural control of energy balance: translating circuits to therapies. *Cell.* 2015;161(1):133-45.
41. Lelliott C, and Vidal-Puig AJ. Lipotoxicity, an imbalance between lipogenesis de novo and fatty acid oxidation. *Int J Obes Relat Metab Disord.* 2004;28 Suppl 4:S22-8.
42. Mayer J. Glucostatic mechanism of regulation of food intake. *N Engl J Med.* 1953;249(1):13-6.
43. Oomura Y, Kimura K, Ooyama H, Maeno T, Iki M, and Kuniyoshi M. Reciprocal Activities of the Ventromedial and Lateral Hypothalamic Areas of Cats. *Science.* 1964;143(3605):484-5.
44. Machler P, Wyss MT, Elsayed M, Stobart J, Gutierrez R, von Faber-Castell A, et al. In Vivo Evidence for a Lactate Gradient from Astrocytes to Neurons. *Cell Metab.* 2016;23(1):94-102.
45. Leen WG, Wevers RA, Kamsteeg EJ, Scheffer H, Verbeek MM, and Willemsen MA. Cerebrospinal fluid analysis in the workup of GLUT1 deficiency syndrome: a systematic review. *JAMA Neurol.* 2013;70(11):1440-4.
46. Garcia-Caceres C, Quarta C, Varela L, Gao Y, Gruber T, Legutko B, et al. Astrocytic Insulin Signaling Couples Brain Glucose Uptake with Nutrient Availability. *Cell.* 2016;166(4):867-80.
47. Gruber T, Pan C, Contreras RE, Wiedemann T, Morgan DA, Skowronski AA, et al. Obesity-associated hyperleptinemia alters the gliovascular interface of the hypothalamus to promote hypertension. *Cell Metab.* 2021;33(6):1155-70 e10.
48. Guillebaud F, Duquenne M, Djelloul M, Pierre C, Poirot K, Roussel G, et al. Glial Endozepines Reverse High-Fat Diet-Induced Obesity by Enhancing Hypothalamic Response to Peripheral Leptin. *Mol Neurobiol.* 2020;57(8):3307-33.

49. Nuzzaci D, Cansell C, Lienard F, Nedelec E, Ben Fradj S, Castel J, et al. Postprandial Hyperglycemia Stimulates Neuroglial Plasticity in Hypothalamic POMC Neurons after a Balanced Meal. *Cell Rep.* 2020;30(9):3067-78 e5.
50. Guillebaud F, Barbot M, Barbouche R, Brezun JM, Poirot K, Vasile F, et al. Blockade of Glial Connexin 43 Hemichannels Reduces Food Intake. *Cells.* 2020;9(11).
51. Kotini M, Barriga EH, Leslie J, Gentzel M, Rauschenberger V, Schambony A, et al. Gap junction protein Connexin-43 is a direct transcriptional regulator of N-cadherin in vivo. *Nat Commun.* 2018;9(1):3846.
52. Yaswen L, Diehl N, Brennan MB, and Hochgeschwender U. Obesity in the mouse model of pro-opiomelanocortin deficiency responds to peripheral melanocortin. *Nat Med.* 1999;5(9):1066-70.
53. Challis BG, Coll AP, Yeo GS, Pinnock SB, Dickson SL, Thresher RR, et al. Mice lacking pro-opiomelanocortin are sensitive to high-fat feeding but respond normally to the acute anorectic effects of peptide-YY(3-36). *Proc Natl Acad Sci U S A.* 2004;101(13):4695-700.
54. Huszar D, Lynch CA, Fairchild-Huntress V, Dunmore JH, Fang Q, Berkemeier LR, et al. Targeted disruption of the melanocortin-4 receptor results in obesity in mice. *Cell.* 1997;88(1):131-41.
55. Zheng H, Patterson LM, Phifer CB, and Berthoud HR. Brain stem melanocortinergic modulation of meal size and identification of hypothalamic POMC projections. *Am J Physiol Regul Integr Comp Physiol.* 2005;289(1):R247-58.
56. Zhan C, Zhou J, Feng Q, Zhang JE, Lin S, Bao J, et al. Acute and long-term suppression of feeding behavior by POMC neurons in the brainstem and hypothalamus, respectively. *J Neurosci.* 2013;33(8):3624-32.
57. Cortes-Campos C, Elizondo R, Carril C, Martinez F, Boric K, Nualart F, et al. MCT2 expression and lactate influx in anorexigenic and orexigenic neurons of the arcuate nucleus. *PLoS One.* 2013;8(4):e62532.
58. Quinones M, Hernandez-Bautista R, Beiroa D, Heras V, Torres-Leal FL, Lam BYH, et al. Sirt3 in POMC neurons controls energy balance in a sex- and diet-dependent manner. *Redox Biol.* 2021;41:101945.
59. Al-Massadi O, Quinones M, Clasadonte J, Hernandez-Bautista R, Romero-Pico A, Folgueira C, et al. MCH Regulates SIRT1/FoxO1 and Reduces POMC Neuronal Activity to Induce Hyperphagia, Adiposity, and Glucose Intolerance. *Diabetes.* 2019;68(12):2210-22.
60. Messina A, Langlet F, Chachlaki K, Roa J, Rasika S, Jouy N, et al. A microRNA switch regulates the rise in hypothalamic GnRH production before puberty. *Nat Neurosci.* 2016;19(6):835-44.
61. Tschop MH, Speakman JR, Arch JR, Auwerx J, Bruning JC, Chan L, et al. A guide to analysis of mouse energy metabolism. *Nat Methods.* 2012;9(1):57-63.
62. Denis RG, Joly-Amado A, Webber E, Langlet F, Schaeffer M, Padilla SL, et al. Palatability Can Drive Feeding Independent of AgRP Neurons. *Cell Metab.* 2015;22(4):646-57.

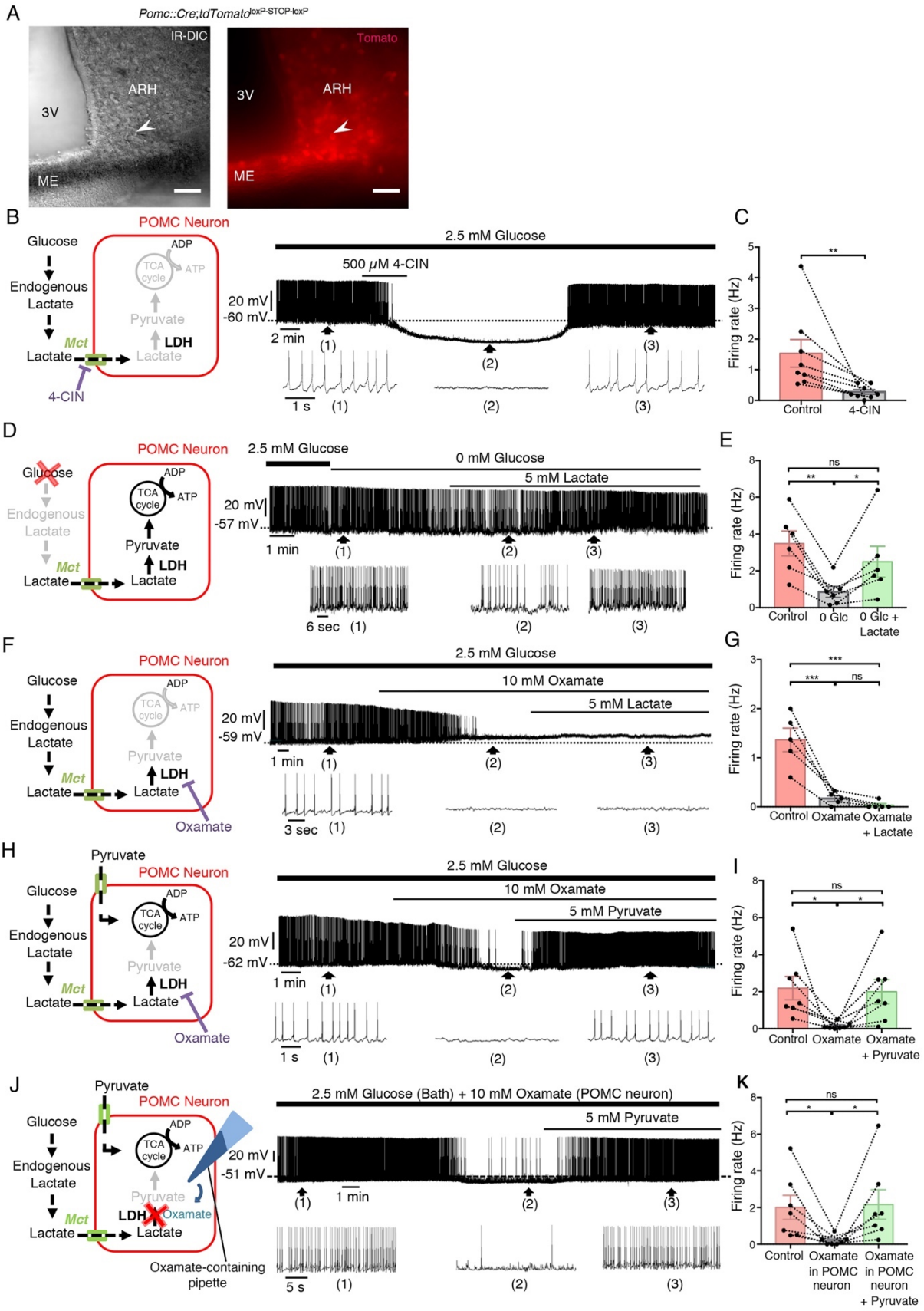


Figure 1. Endogenous production of lactate sustains the activity of POMC neurons.

(A1 and A2) Infrared differential interference contrast (IR-DIC) image of the arcuate nucleus (ARH) at the level of the median eminence (ME) showing a patch-clamp electrode placed onto the cell body of a POMC neuron (A1) identified via fluorescence (A2) in a tdTomato^{POMC} mouse. 3V: third ventricle. Scale bar, 50 μm.

(B) Schematic model representing the modulation of POMC neuronal activity by lactate. Whole-cell current-clamp recording of a POMC neuron performed in artificial cerebrospinal fluid (ACSF) containing a physiological concentration of glucose, showing that bath application of α-cyano-4-hydroxycinnamate (4-CIN), an inhibitor of monocarboxylate transporters (MCTs), blunts its spontaneous neuronal activity. Bottom traces show expansions of the recording at the indicated time points 1, 2 and 3. TCA: tricarboxylic acid. LDH: lactate dehydrogenase.

(C) Firing rate of POMC neurons before and after the bath application of 4-CIN.

(**D,E)** Switch in ACSF glucose concentrations from 2.5 to 0 mM decreases the spontaneous firing rate of POMC neurons. In the same neuron, lactate reverses the glucose deprivation effect.

(F) Inhibiting LDH with oxamate inhibits spontaneous POMC neuronal activity in ACSF with 2.5 mM glucose. Lactate, the substrate of LDH, does not reverse the inhibitory effect of oxamate on the same neuron.

(G) Lack of compensation by lactate of the inhibitory effect of oxamate on the firing rate of POMC neurons.

(H,I) Bath application of LDH inhibitor, oxamate, inhibits the activity of POMC neurons in ACSF with 2.5 mM glucose. In the same neuron, pyruvate, the metabolite of LDH, reverses the inhibitory effect of oxamate.

(J,K) Intracellular application of oxamate in POMC neurons inhibits their activity in ACSF with 2.5 mM glucose. In the same neuron, the bath application of pyruvate reverses the inhibitory effect of oxamate. *P<0.05, ** P<0.01, *** P<0.001, ns: non-significant.

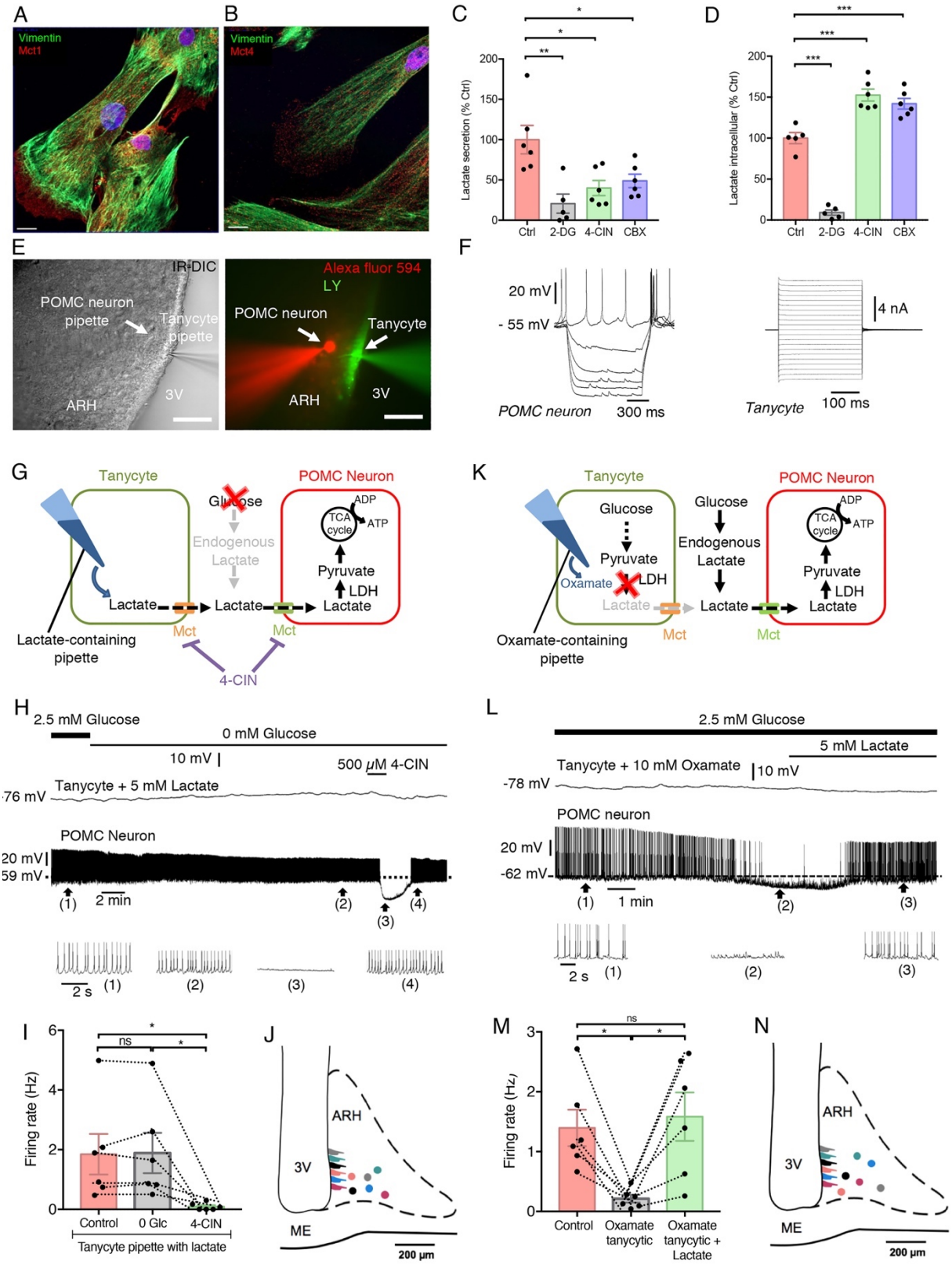


Figure 2. Lactate supply in tanycytes sustains the activity of POMC neurons.

(A and **B)** Representative image showing, vimentin (green, **A**,**B**), monocarboxylate transporter 1 (MCT1) (red, **A**) and monocarboxylate transporter 4 (MCT4) (red, **B**) immunoreactivities in primary cultures of tanycytes. Blue shows DAPI counterstaining (blue; **B**). Scale bar, 10μm.

(C) Lactate secretion in cultured tanycyte exposed to different conditions (no treatment [ctrl], 2-deoxyglucose [2-DG], carbenoxolone [CBX], α-cyano-4-hydroxycinnamate [4-CIN]).

(D) Intracellular lactate in cultured tanycyte exposed to different conditions.

(E) Infrared differential interference contrast (IR-DIC, left panel) and fluorescence (Right panel) images of the ARH at the level of the ME showing recording from a paired tanycyte and POMC neuron (dyad), filled with Lucifer yellow (LY, green) and Alexa Fluor-594 (red), respectively. 3V: third ventricle. Scale bar, 50μm. *Right panel*.

(F) Responses of a POMC neuron and an ARH tanycyte to a current modulation from -50pA to 0pA with a step of 10pA and a duration of 1s, and to a voltage modulation from -100mV to 100mV with a step of 10mV and a duration of 300ms, respectively.

(G-J) Schematic model (**G**) and representative recording (**H**) of an ARH tanycyte-POMC neuron dyad (**J**) in whole-cell patch-clamp mode showing that dialyzing tanycyte with 5mM lactate prevents the inhibitory effect of exogenous glucose deprivation (0mM glucose) on neuronal firing (**H**,**I**). In the same neuron, the inhibition of MCTs by the bath application of 4-CIN cancels this effect (**H**,**I**). LDH: Lactate dehydrogenase. TCA: tricarboxylic acid.

(K-N) Schematic model (**K**) and representative recording (**L**) of an ARH tanycyte-POMC neuron dyad (**N**) in whole-cell patch-clamp mode showing that dialyzing the tanycyte with 10mM oxamate inhibits POMC neuronal firing (**L**,**M**). In the same neuron, this inhibition is compensated for by the bath application of 5mM lactate (**L**,**M**).

P*<0.05, ** *P*<0.01, * *P*<0.001, ns: non-significant.

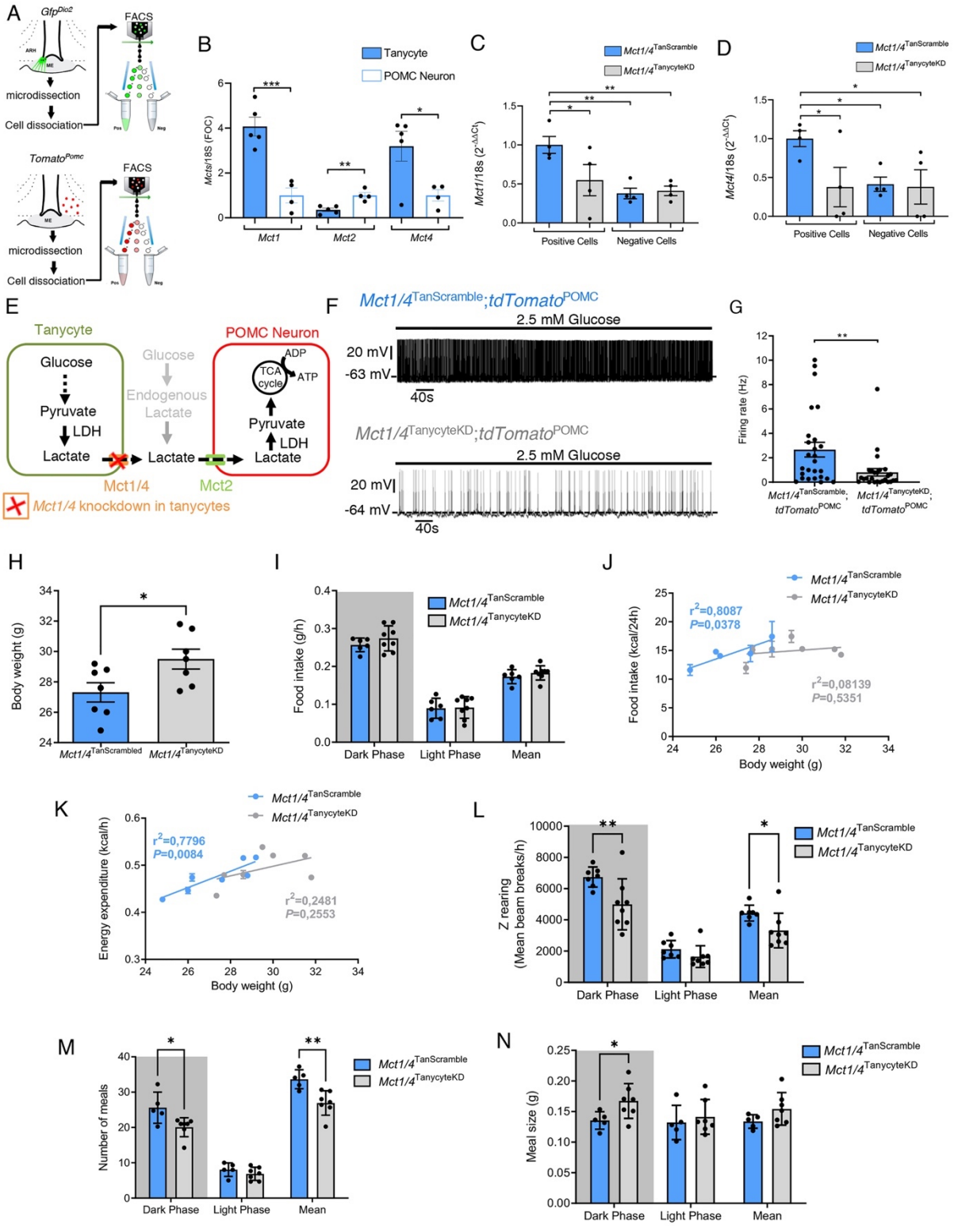


Figure 3: Inhibition of lactate transport in tanycytes alters energy balance.

(A) Schematic model for fluorescence-activated cell sorting (FACS) used to isolate putative GFP- and Tomato-positive tanycytes and POMC neurons, respectively.

(B) Relative monocarboxylate transporter expression (*Mct1*, *Mct2* and *Mct4*) in tanycytes and POMC neurons (gene expression levels were normalized to the level in POMC neurons, arbitrarily set at 1. See also Figure S2 for the characterization of sorted cells.

(C and **D)** *Mct1* (**C**) and *Mct4* (**D**) mRNA expression levels, in GFP-positive and -negative cells in both *Mct1/4*^{TanScramble} and *Mct1/4*^{TanycyteKD} mice.

(E) Schematic model representing the inhibition of *Mct1* and *Mct4* in tanycytes.

(F) Whole-cell current-clamp recordings performed in ACSF containing 2.5 mM glucose showing the spontaneous firing rate of a POMC neuron from an *Mct1/4*^{TanycyteKD} mouse and another from an *Mct1/4*^{TanScramble} mouse.

(G) Comparison of firing rates of POMC neurons between *Mct1/4*^{TanScramble} and *Mct1/4*^{TanycyteKD} mice.

(H) Bar graph representing body weight in *Mct1/4*^{TanScramble} and *Mct1/4*^{TanycyteKD} mice.

(I) Bar graph representing food intake during the dark and light phases in *Mct1/4*^{TanScramble} and *Mct1/4*^{TanycyteKD} mice.

(J) Linear regression between food intake and body weight in *Mct1/4*^{TanScramble} and *Mct1/4*^{TanycyteKD} mice.

(K) Linear regression between energy expenditure and the body weight in MCT-1/4^{Scrambled} and MCT-1/4^{TanycyteKD} mice.

(L-N) Bar graphs representing Z rearing (**L**), number of meals (**M**) and meal size (**N**), during the dark and light phase, in *Mct1/4*^{TanScramble} and *Mct1/4*^{TanycyteKD} mice.

* $P<0.05$, ** $P<0.01$, *** $P<0.001$.

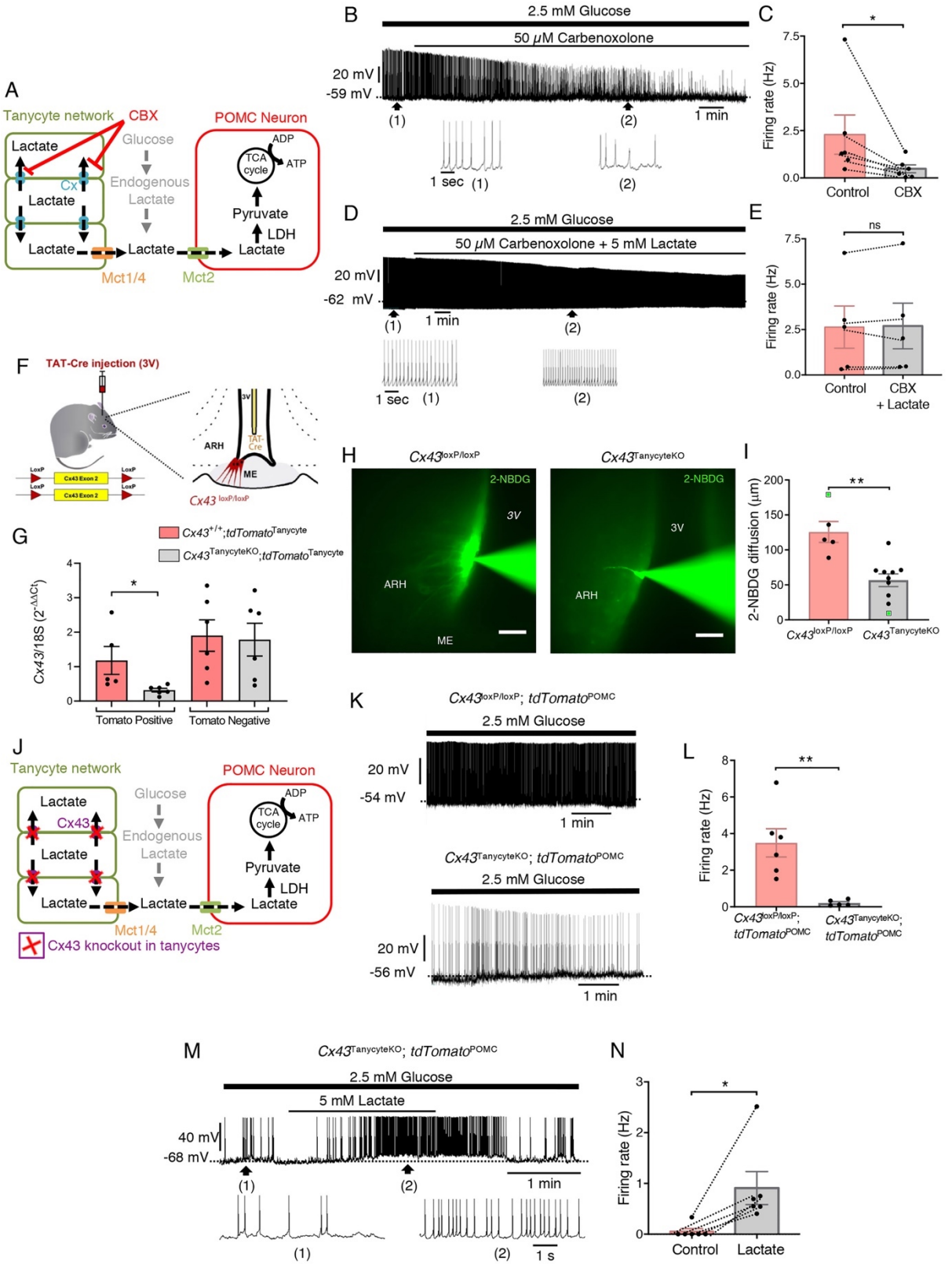


Figure 4. Lactate trafficking through the tanycytic network is necessary to sustain the activity of POMC neurons.

(A) Schematic model representing the involvement of the tanycytic network in shuttling lactate to POMC neurons. CBX, carbenoxolone; Cx, connexins.

(B, E) Representative whole-cell current-clamp recording of a POMC neuron (**B**,**D**) in ACSF containing a physiological concentration of glucose (2.5 mM), showing that the bath application of CBX decreases the spontaneous firing rate of the neuron (**B**,**C**) and that bath application of lactate reverses this effect (**D**,**E**).

(F) $Cx43^{TanycyteKO}$ model. The tanycyte-specific deletion of connexin 43 (Cx43) was carried out by infusing the TAT-Cre fusion protein into the third ventricle (3V) of $Cx43^{loxP/loxP}$ mice.

(G) mRNA expression levels for *Cx43* in Tomato-positive and -negative cells, in $Cx43^{+/+}$ and $Cx43^{TanycyteKO}$ mice.

(H,I) Illustration of the maximal and minimal diffusion through ARH tanycytes of the fluorescent glucose analog 2-[N-(7-notrobenz-2-oxa-1,3-diazol-4-y)amino]-2-deoxyglucose (2-NBDG; green) injected into a single tanycyte in a control $Cx43^{loxP/loxP}$ and a $Cx43^{TanycteKO}$ mouse, respectively, via a patch pipette for 20 minutes (**H**), corresponding to the two animals highlighted in green in (**I**). Scale bar, 50 μm.

(J) Schematic model representing the involvement of a tanycytic network mediated by Cx43 gap junctions in lactate shuttling to POMC neurons. This model was tested by recording the electrical activity of POMC neurons in $Cx43^{TanycyteKo}$ mice.

(K,L) Representative whole-cell current-clamp recording performed in ACSF containing 2.5 mM glucose showing the spontaneous firing rate of a POMC neuron from a $Cx43^{loxP/loxP}$;$tdTomato^{POMC}$ (top trace) and a $Cx43^{TanycyteKO}$;$tdTomato^{POMC}$ (top trace) mouse, as quantified in (**L**).

(M,N) Representative whole-cell current-clamp recording of a POMC neuron from a $Cx43^{TanycyteKO}$;$tdTomato^{POMC}$ mouse performed in ACSF containing 2.5 mM glucose showing that the bath application of 5 mM lactate increases its firing rate, as quantified in (**N**).

P*<0.05, ** *P*<0.01, * *P*<0.001, ns: non-significant.

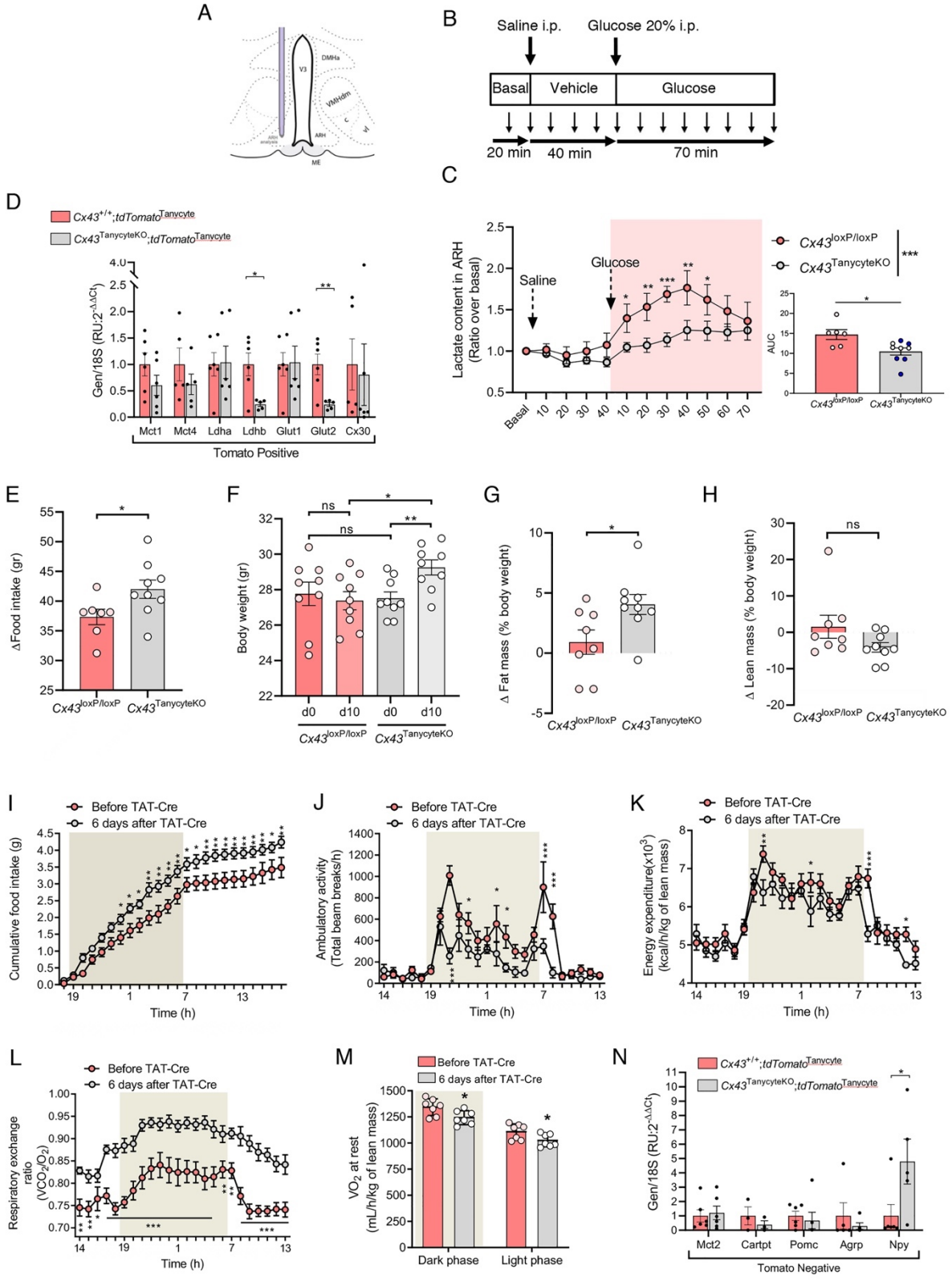


Figure 5. Lactate trafficking in the tanycytic network is necessary to sustain energy homeostasis.

(A-C) Lactate levels in the mediobasal hypothalamus (**C**) assessed using microdialysis (**A**) in Cx43^{TanycyteKO} mice compared to *Cx43*$^{loxP/loxP}$ mice, before (basal) and after an intraperitoneal (i.p.)

injection of saline followed by glucose (2 mg/kg body weight) **(B)**. The bar graph in (**C**) represents the area under the curve (AUC) during glucose treatment in *Cx43*$^{loxP/loxP}$ mice or Cx43^{TanycyteKO} littermates, in which gene recombination was either induced by infusing the recombinant TAT-Cre protein into the third ventricle (n=4, light dots) or injecting the AAV1/2 *Dio2::Cre* into the lateral ventricle (n=5, dark dots).

(D) Comparison of mRNA expression levels for *Mct*-1, *Mct4*, *Ldha*, *Ldhb*, *Glut1*, *Glut2* and *Cx30* in Tomato-positive cells between *Cx43*$^{+/+}$;*tdTomato*^{tanycyte} and *CX43*^{TanycyteKO};*tdTomato*^{tanycyte} mice.

(E) Bar graph representing delta food intake between Day 0 and Day 10 following TAT-Cre injection in Cx43^{TanycyteKO} mice compared to Cx43$^{loxP/loxP}$ control mice.

(F) Bar graph representing body weight in Cx43^{TanycyteKO} mice and Cx43$^{loxP/loxP}$ control mice, on Day 0 and on Day 10 following TAT-Cre injection.

(G,H) Bar graphs representing delta fat mass (**G**) and lean mass (**H**) between Day 0 and Day 10 following TAT-Cre injection in Cx43^{TanycyteKO} mice compared to Cx43$^{loxP/loxP}$ control mice.

(I-L) Cumulative food intake **(I)**, Ambulatory activity **(J),** energy expenditure **(K)** and respiratory exchange ratio (RER) (**L)** before and 6 days after TAT-Cre injection into the third ventricle.

(M) Bar graph representing O_2 consumption at rest 6 days after TAT-Cre injection into the third ventricle, during the dark and light phases.

(N) Comparison of mRNA expression levels for *Mct2*, *Cartpt*, *Pomc*, *AgRP* and *Npy* in Tomato-negative cells between Cx43$^{+/+}$ and CX43^{TanycyteKO} mice.

P*<0.05, ** *P*<0.01, * *P*<0.001, ns: non-significant.

SUPPLEMENTARY METHODS

Animals

The experiments used transgenic Cx43$^{loxP/loxP}$, tdTomato^{POMC} and Cx43$^{loxP/loxP}$;tdTomato^{POMC} mice. tdTomato^{POMC} mice were generated by breeding Pomc-Cre mice with ROSA-tdTomato mice. These mice were bred with Cx43$^{loxP/loxP}$ mice, in which exon 2 of the Cx43 allele is flanked by two LoxP sites, to generate Cx43$^{loxP/loxP}$;tdTomato^{POMC} mice. Cx43$^{loxP/loxP}$, Pomc-cre and ROSA-tdTomato mice purchased from The Jackson Laboratories (Bar Harbor, ME; Pomc-cre line: 005965 – STOCK Tg(Pomc1-cre)16Lowl/J, ISMR Cat#JAX:005965, RRID:IMSR_JAX:005965; ROSA-tdTomato line: 007914 – B6.Cg-*Gt(ROSA)26Sor*$^{tm14(CAG-tdTomato)Hze}$/J, ISMR Cat#JAX:007914, RRID:IMSR_JAX007914; Cx43$^{loxP/loxP}$ line: 008039 – B6.129S7-*Gja1*^{tm1Dig}/J, IMSR Cat#JAX:008039, RRID_JAX008039). All three lines were maintained on a C57Bl6 background. *Cx43*$^{+/+}$;*tdTomato*$^{loxp\text{-}STOP\text{-}loxP}$ mice were generated by crossing *Cx43*$^{+/loxP}$;*tdTomato*$^{loxp\text{-}STOP\text{-}loxP}$ males with *Cx43*$^{+/loxP}$;*tdTomato*$^{loxp\text{-}STOP\text{-}loxP}$ females. In addition, wild-type C57Bl/6J (Stock No: 000664, B6, Jackson Laboratory) were also used for infection with viral vectors. All mice were bred and housed in a temperature- and humidity-controlled room on a 12h/12h light/dark cycle and with access to food and water ad libitum. Animal studies were performed with the approval of the Institutional Ethics Committees for the Care and Use of Experimental Animals of the University of Lille and the French Ministry of National Education, Higher Education and Research (APAFIS#2617-2015110517317420 v5), and under the guidelines defined by the European Union Council Directive of September 22, 2010 (2010/63/EU).

Lactate production and release assay in primary cultures of tanycytes

For lactate release/secretion assays, primary cultures of tanycytes were incubated in ACSF for 2h, then treated with either 2-desoxy-glucose (2-DG, 50 mM, Sigma Cat#D8375, CAS:154-17-6), 4-CIN (500 µM) or CBX (50 µM) for 30 minutes before cell lysis and medium sampling. Lactate concentrations in cell lysates and medium samples were analyzed using the Lactate-Glo™ assay (Promega) following kit instructions.

Isolation of tanycytes and POMC-expressing cells by fluorescence-activated cell sorting (FACS).

For the isolation of POMC-expressing cells, the mediobasal hypothalamus of *tdTomato*^{POMC} mice was microdissected under a stereomicroscope and enzymatically dissociated using a Papain Dissociation System (Worthington, Lakewood, NJ) to obtain a single-cell suspension.

For isolation of tanycytes, two weeks after the injection into the lateral ventricle of AAV1/2 vectors expressing EGFP (Dio2:EGFP or Cre-mediated expression of Mct1/4 shRNAs and EGFP), the median eminence was microdissected under a stereomicroscope and dissociated using a Papain Dissociation System (Worthington, Lakewood, NJ) to obtain a single-cell suspension. FACS was performed using a BD ARIA SORTER and FACSDiva software v8.0.3 (BD Biosciences, Inc). Sorting parameters were based on measurements of Tomato fluorescence (excitation 561nm; detection: bandpass 675+/-20nm) or GFP fluorescence (excitation: 488 nm; detection: GFP bandpass 530+/-30 nm), by comparing cell suspensions from Tomato-positive and wild-type animals. For each animal, 2000 Tomato-positive, 2000 GFP-positive and 2000 Tomato-negative cells were sorted directly into 10 µl of lysis buffer (0.1% Triton® X-100 and 0.4 unit/µl RNaseOUT™ (Life Technologies)) to perform qPCR.

Quantitative qPCR analyses

For gene expression analyses, total RNA obtained from FACS-sorted Tomato-positive, GFP-positive and negative cells was reverse transcribed using High-capacity cDNA Reverse transcription kit (Applied Biosystems™ ref 4368814) after a DNAse treatment (DNase I, Amplification Grade, Invitrogen™, ref 18068015). A linear preamplification step was performed using the TaqMan® PreAmp Master Mix Kit protocol (Applied Biosystems™ ref 4488593). Next, real-time PCR was carried out on an Applied Biosystems 7900HT Fast Real-Time PCR System using the TaqMan® probes listed in Table S1 and TaqMan™ Universal Master Mix II (Applied Biosystems™ ref 4440049). The control housekeeping gene r18S was used for normalization. Gene expression data were analyzed using the $2^{-\Delta\Delta Ct}$ method to compare between negative and positive FACS-sorted cells.

Dye-coupling analysis

After electrophysiological recordings, slices were immediately fixed with 4% paraformaldehyde (PFA) overnight at 4°C. After several washes in phosphate buffered saline (PBS) solution, slices were treated with Alexa Fluor 488 streptavidin (1:250; Invitrogen) with 0.5% Triton X-100 in PBS overnight at 4°C. After rinsing several times in PBS solution, slices were incubated with Hoechst 33342 (1:10,000) for 1 minute. In some experiments, biocytin detection was combined with immunolabeling for the neuronal nuclear marker (NeuN). In this case, slices were incubated with a primary mouse anti-NeuN antibody (1:1000; Millipore, Cat#MAB377, RRID:AB_2298772) in Triton/normal goat serum (NGS)/PBS for 3 days at 4°C, washed several times, then treated with a secondary goat anti-mouse Alexa Fluor 546

antibody (1:500; Invitrogen, Invitrogen Cat#A-11030; RRID: AB_2534089) and Alexa Fluor 488 streptavidin in Triton/NGS/PBS overnight at 4°C. After several rinses with PBS solution, slices were mounted on slides with Mowiol. Images were captured using an Axio Imager Z2 Apotome microscope.

Immunochemistry

For immunocytofluorescence in tanycyte primary cultures, tanycytes were seeded onto poly-L-lysine coated glass coverslips. Cells were fixed for 15 minutes in 4% PFA in PBS, washed three times with PBS and stored at 4°C in PBS-Na azide 0.02%. After three washes with PBS, cells were permeabilized in PBS-Triton 0.25% (PBS-T) for 15 minutes, washed three times with PBS and incubated in a blocking solution of PBS-T BSA 1% for 30 minutes. After blocking, tanycytes were incubated with primary antibodies (Cx43, Millipore Cat#AB1727, RRID:AB_2294609, 1:200; MCT-1, Millipore Cat#AB1286, RRID:AB_11212410, 1:100; MCT-4, Millipore, 1:200; Vimentin, Millipore Cat#AB3314P, RRID:AB_2286063, 1:1000; Vimentin, DAKO Cat#M0725, RRID:AB_10013485, 1:100) in blocking solution overnight at 4°C. Cells were then washed 3 times with PBS and incubated with secondary antibodies in PBS-T for 1 hour at room temperature. After three PBS washes, cells were incubated with DAPI (1:5000, Sigma Cat#D9542, CAS:28718-90-3) for 5 minutes at room temperature and washed three times with PBS. Images were captured using an Axio Imager Z2 Apotome microscope.

For immunohistochemical detection, mice were deeply anesthetized with 50-100 mg/kg of ketamine hydrochloride and xylazine hydrochloride and perfused via the left ventricle with 20 ml PBS solution followed sequentially by 100 ml of 4% PFA in 0.1 M PBS, pH 7.4. Brains were rapidly removed and postfixed in 4% PFA for 24 hours at 4°C. After fixation, they were cryoprotected by immersing for 24 hours in a solution of 30% sucrose in PBS. Coronal 40 μm-thick hypothalamic sections containing the arcuate nucleus were cut serially at 200 μm intervals on a freezing microtome (SM2010R; Leica) and then stored in an antifreeze solution at -20°C until immunolabeling. To determine tanycytic Cx43 expression, double immunofluorescence labeling for Cx43 and vimentin was performed on free-floating sections. Sections were incubated with 5% normal goat serum (NGS), 0.3% triton X-100 in 0.1 M PBS blocking solution for 1 hour at room temperature, then with primary mouse anti-Cx43 (1:500; Millipore) and chicken anti-vimentin antibodies (1:2000; Millipore Cat#AB5733, RRID:AB_11212377), or rabbit anti-POMC propeptide (1:200; Phoenix pharmaceuticals, Cat#H02930, RRID:AB_2307442), and a chicken anti-GFP (1:1000; Invitrogen, Cat#A10262, RRID:AB_2534023) overnight at 4°C on a shaking

platform. After several washes in PBS, sections were treated with secondary goat anti-mouse Alexa Fluor 546 (1:1000; Invitrogen, Cat#A-11030, RRID:AB_2534089) and goat anti-chicken Alexa Fluor 633 (1:500; Invitrogen Cat##A-21103, RRID:AB_2535756). All sections were counterstained with Hoechst 33342 (1:10000; Invitrogen Cat#H3570, CAS:23491-52-3), and mounted on slides with Mowiol. Immunofluorescence images were captured using an LSM 710 Zeiss confocal microscope.

SUPPLEMENTARY TABLE

Taqman probe	Gene	
Mm00475829_g1	Agrp	Agouti-related peptide
Mm04210469_m1	Cartpt	Cocaine- and amphetamine-regulated transcript protein
Mm00515664_m1	Dio2	Iodothyronine deiodinase 2
Mm01151962_m1	Elavl3	ELAV-like protein 3 (Hu-antigen C, HuC)
Mm00439129_m1	Gck	Glucokinase
Mm01179639_s1	Gja1	Cx43
Mm00433661_s1	Gjb6	Cx30
Mm00439147_m1	Gpr50	Melatonin-related receptor (G protein-coupled receptor 50) (H9)
Mm01612132_g1	Ldh1	Lactate dehydrogenase a
Mm05874166_g1	Ldh5	Lactate dehydrogenase b
Mm01410146_m1	NPY	Neuropeptide Y
Mm00435874_m1	POMC	Pro-opiomelanocortin
Mm00454892_m1	Ppp1r1b	Darpp32
Mm03928990_g1	Rn18s	Ribosomal 18S
Mm01306379_m1	Slc16a1	Mct1, solute carrier family 16 (monocarboxylic acid transporters), member 1
Mm00446102_m1	Slc16a3	Mct4, solute carrier family 16 (monocarboxylic acid transporters), member 3
Mm00441442_m1	Slc16a7	Mct2, solute carrier family 16 (monocarboxylic acid transporters), member 7
Mm00441480_m1	Slc2a1	Glut1
Mm00446229_m1	Slc2a2	Glut2
Mm00436615_m1	Slc2a4	Glut4
Mm01333430_m1	Vim	Vimentin

Table S1. Taqman probes used for qPCR.

SUPPLEMENTARY FIGURES

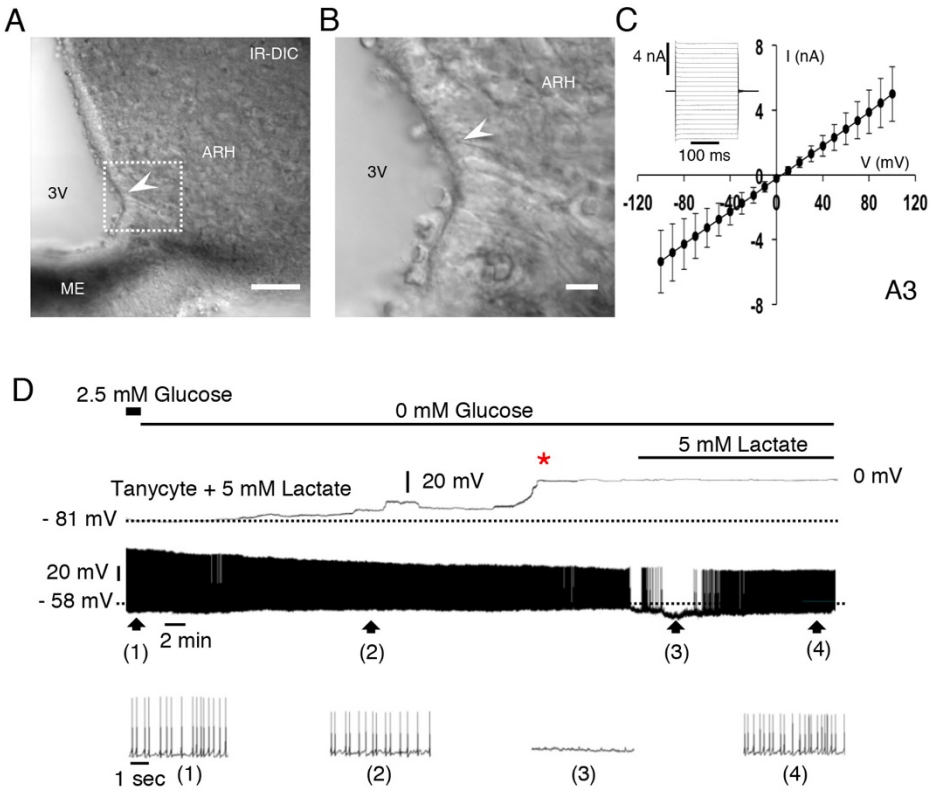


Figure S1. Intracellular lactate delivery to tanycytes maintains the electrical activity of POMC neurons during exogenous glucose deprivation.

(A) Infrared differential interference contrast (IR-DIC) image of an arcuate nucleus (ARH) slice (250 µm-thick) at the level of the median eminence (ME). 3V: third ventricle. Scale bar, 50 µm.

(B) Higher magnification of the area delineated by the white square in (A1) showing the strip of ARH tanycytic cell bodies (arrowhead) lining the wall of the third ventricle (3V) and a single process (arrowhead) extending into the ARH. Scale bar, 20 µm.

(C) Representative membrane current of an ARH tanycyte in response to voltage pulses and average I(V) curve for ARH tanycytes (n=8 cells).

(D) Recording of a paired ARH tanycyte and POMC neuron (dyad) in whole-cell patch-clamp mode showing that filling the tanycyte with 5 mM lactate allows the electrical activity of a POMC neuron to be maintained during exogenous glucose deprivation (0 mM), and that the loss of the patched tanycyte, represented by the red asterisk, leads to a decrease in the firing rate of the neuron that can be

compensated by the bath application of 5 mM lactate. Bottom traces show expansions of the recording at the indicated time points 1, 2, 3 and 4.

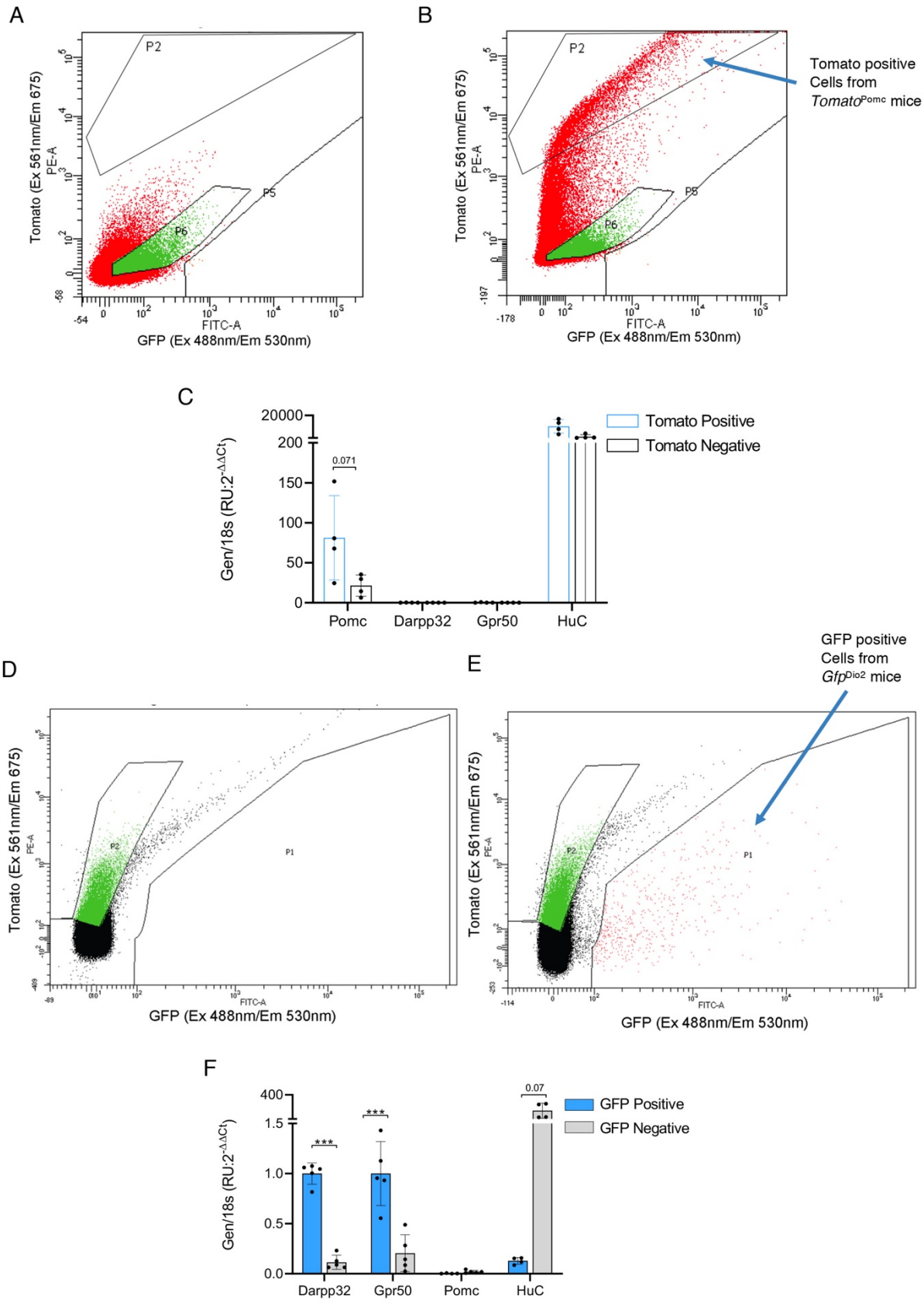

A
B
P2
P5
P6
Tomato (Ex 561nm/Em 675)
PE-A
FITC-A
GFP (Ex 488nm/Em 530nm)
Tomato positive
Cells from
Tomato^Pomc mice
C
Gen/18s (RU:2^-ΔΔCt)
0.071
Tomato Positive
Tomato Negative
Pomc
Darpp32
Gpr50
HuC
D
E
P1
GFP positive
Cells from
Gfp^Dio2 mice
F
***
0.07
GFP Positive
GFP Negative

Figure S2. FACS and qPCR analyses in mice in wild-type mice selectively expressing tdTomato and green fluorescent protein (GFP) in POMC neurons and tanycytes, respectively.

(A and **B)** Gating strategy for sorting Tomato-positive putative POMC neurons from *Pomc::cre*; *tdTomato*$^{loxP\text{-}STOP\text{-}loxP}$ mice.

(C) mRNA expression levels of control markers in Tomato-positive and -negative cells (unpaired student's t-tests; *Pomc*, P=0.071; *Darpp32*, P=0.158; *Gpr50*, P=0.319; *Huc*, P=0.027; n=4 mice).

(D and **E)** Gating strategy for sorting GFP expressing cells.

(F) mRNA expression levels of tanycytic markers in GFP-positive and -negative cells (unpaired Student's t-tests; *Darpp32*, P<0.001; *Gpr50*, P=0.001; *Pomc*, P=0.06; *Huc*, P=0.07; n=5 mice).

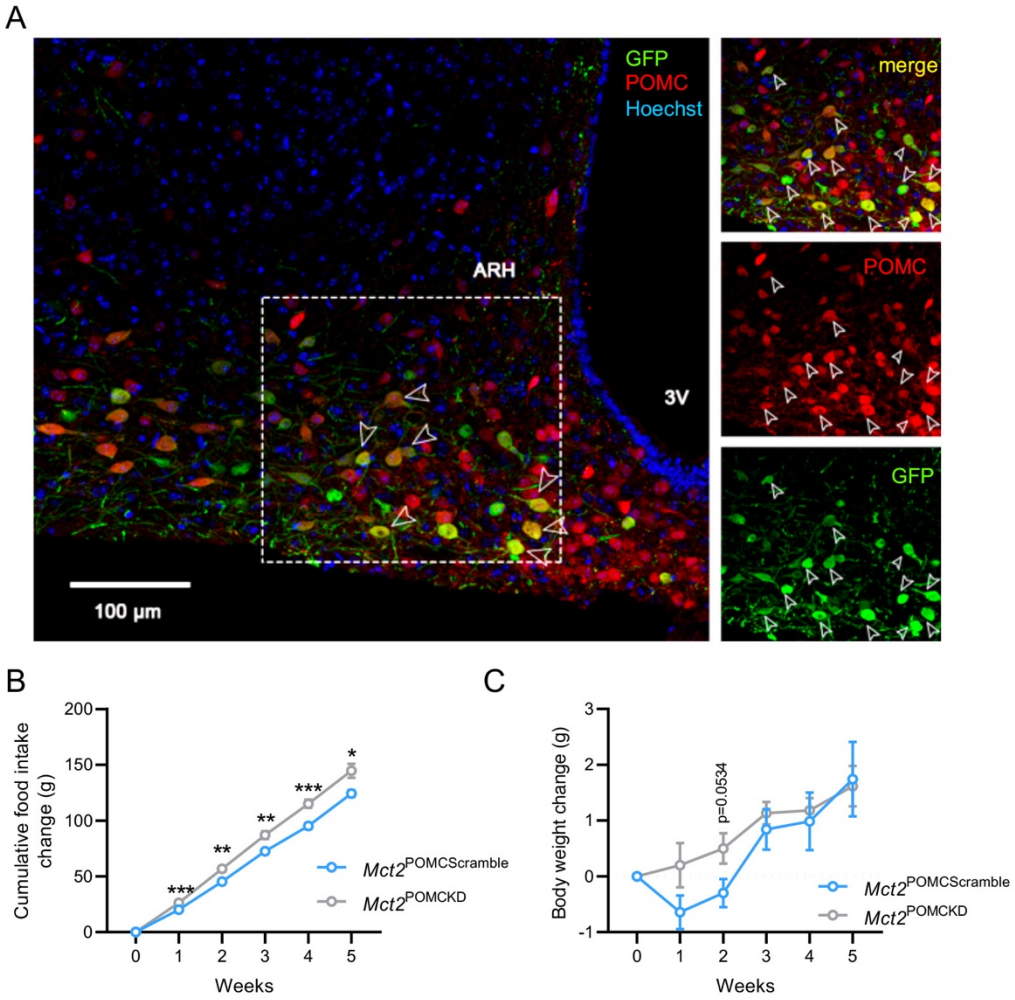


Figure S3. Effect of selectively knocking down Mct2 expression in POMC neurons on cumulative food intake and body weight.

(A) Immunofluorescence image showing that GFP transgene expression (green) was restricted to POMC neurons (red) in *Pomc::cre* mice injected into the arcuate nucleus of the hypothalamus (ARH) with AAV8 expressing shRNA:GFP in a Cre-dependent manner.

(B and C) Effect of the viral-vector-induced knockdown of *Mct2* expression selectively in POMC neurons (*Mct2*^{POMCKD}) on cumulative food intake (B) and the body weight (C) in male mice compared to mice expressing a scrambled shRNA in POMC neurons (*Mct2*^{POMCScramble}) (unpaired Student's t-tests; (B), Week 1, *P*=0.0003; Week 2, *P*=0.0018; Week 3, *P*=0.0045; Week 4, *P*=0.0008; Week 5, *P*=0.0114; (C), Week 1, *P*=0.1135; Week 2, *P*=0.0534; Week 3, *P*=0.5188; Week 4, *P*=0.7470; Week 5, *P*=0.8773; n=7 Mct2^{POMCScramble} and 6 Mct2^{POMCKO} mice). * P<0.05, **P<0,01, ***P<0,001.

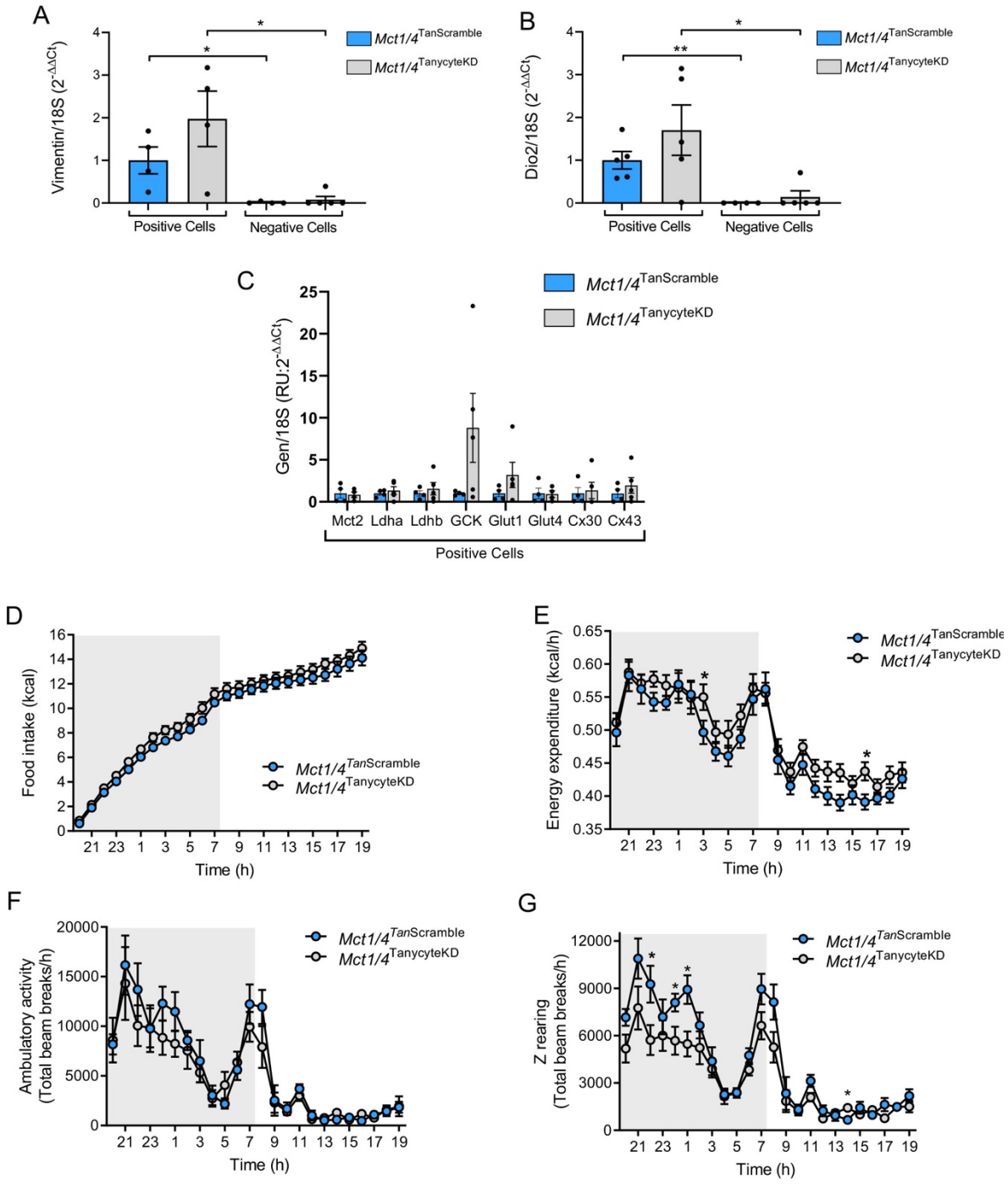


Figure S4. Gene expression and metabolic profiling in mice in which *Mct1* and *Mct4* have been selectively knocked down in *Dio2*-expressing tanycytes.

(A) mRNA expression levels of tanycytic markers, *Vimentin* (A1) and *Dio2* (A2) in GFP-positive and -negative cells (unpaired Student's t-tests; (A1) *Mct1/4*$^{\text{TanScramble}}$/positive cells vs. *Mct1/4*$^{\text{TanScramble}}$/negative cells P=0.0200, *Mct1/4*$^{\text{TanycyteKD}}$/positive cells vs. *Mct1/4*$^{\text{TanycyteKD}}$/negative

cells, *P*=0.0134; (A2) *Mct1/4*$^{\text{TanScramble}}$/positive cells vs. *Mct1/4*$^{\text{TanScramble}}$/negative cells *P*=0.0037, *Mct1/4*$^{\text{TanycyteKD}}$/positive cells vs. *Mct1/4*$^{\text{TanycyteKD}}$/negative cells, *P*=0.0324; n=4 mice). **P*<0.05.

(B) Real-time PCR analysis for various gene transcripts (*Mct2*, *Ldha*, *Ldhb*, Glucokinase (*Gck*), *Glut1*, *Glut4*, *Cx30* and *Cx43*) in GFP-positive cells, between *Mct1/4*$^{\text{TanScramble}}$ and *Mct1/4*$^{\text{TanycyteKD}}$ mice (unpaired Student's tests; *Mct2*, *P*=0.8204; *Ldha*, *P*=0.5561; *Ldhb*, *P*=0.5457, *Gck, P*=0.1381; *Glut1*, *P*=0.2479; *Glut4*, *P*=0.9174; *Cx30*, *P*=0.7825; *Cx43*, *P*=0.4315; n=6 mice).

(D-G) Cumulative food intake (**D**), energy expenditure (**E**), ambulatory activity (**F**) and Z rearing (**G**) in *Mct1/4*$^{\text{TanScramble}}$ and *Mct1/4*$^{\text{TanycyteKD}}$ mice (two-way ANOVA followed by an uncorrected Fisher's LSD test; **D**, *P*=0.2310, n=6 and 8 mice; **E**, *P*=0.04480, n=7 and 8 mice; **F**, *P*=0.5215, n=7 and 8 mice; **G**, *P*=0.0305, n=7 and 8 mice). **P*<0.05.

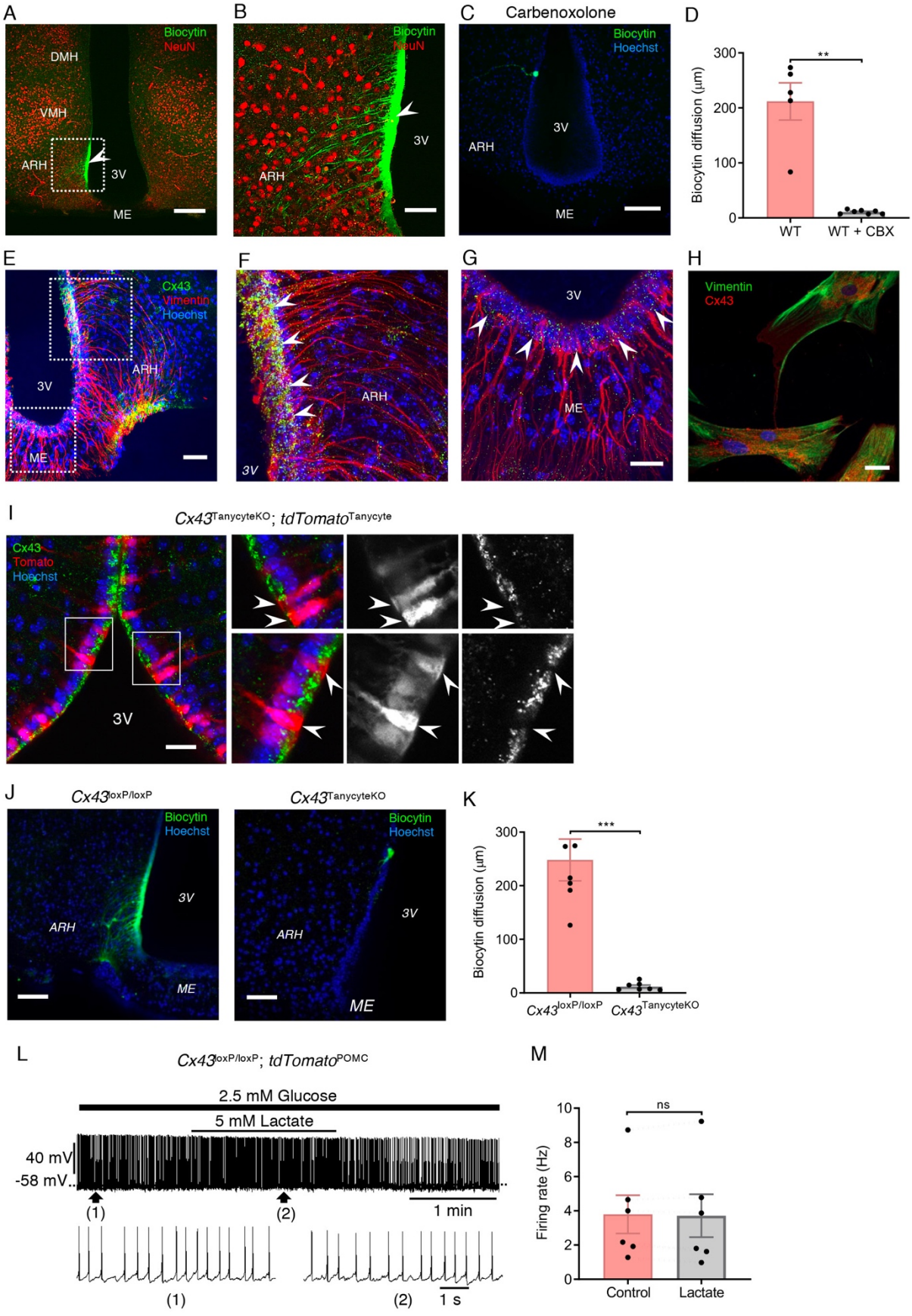


Figure S5. ARH tanycytes form a network of cells interconnected by connexin 43 gap junctions.

(A) Extensive intercellular dye-coupling between ARH tanycytes visible after fixation of the WT hypothalamic slice and revelation of biocytin by fluorochrome-conjugated streptavidin (green), combined with immunofluorescence labeling for NeuN (red). The arrow indicates the single tanycyte that was recorded for 20 minutes with a whole-cell patch-clamp electrode containing biocytin. DMH: dorsomedial hypothalamus. VMH: ventromedial hypothalamus. Scale bar, 200 μm.

(B) Higher magnification of the area delineated by the white square in (B1). Scale bar, 100 μm.

(C) Treatment of a WT slice with the gap-junction blocker carbenoxolone (CBX, 50 μM) abolished the intercellular diffusion of biocytin (green) between ARH tanycytes.

(D) Extent of biocytin diffusion in WT slices and slices treated with CBX. Statistical differences were tested using a Mann-Whitney U test (WT vs. WT+ CBX, U=0, P=0.0025; n=5 and 7 cells, 4 and 5 mice). ** P<0.01.

(E) Confocal image of a hypothalamic section showing Hoechst nuclear staining (blue), Cx43 immunolabeling (green) and vimentin immunolabeling (red) in the arcuate nucleus of the hypothalamus (ARH) and the median eminence (ME). 3V: third ventricle. Scale bar, 50 μm.

(F and **G)** Higher magnification of the ARH (**F**) and ME (**G**) regions delineated by white squares in (**E**), showing the dense punctiform expression of Cx43 in the cell bodies of ARH tanycytes lining the 3V (**F**, arrowheads) compared to almost non-existent labeling in the cell bodies of ME tanycytes (B3, arrowheads). Scale bar, 25 μm.

(H) Primary cultures of tanycytes immunolabeled with anti-connexin 43 (Cx43) antibody and anti-vimentin antibodies and counterstained with DAPI to reveal cell nuclei. Scale bar, 10 μm.

(I) Confocal image of a hypothalamic section showing Cx43 immunolabeling (green), tdTomato expression (red) and Hoechst staining (blue) in *Cx43*$^{\text{TanycyteKO}}$;tdTomato mice. Scale bar, 25 μm.

(J) Representative diffusion of biocytin through ARH tanycytes in *Cx43*$^{\text{loxP/loxP}}$ and *Cx43*$^{\text{TanycyteKO}}$ slices. Scale bar, 50 μm.

(K) Extent of biocytin diffusion in *Cx43*$^{\text{loxP/loxP}}$ and *Cx43*$^{\text{TanycyteKO}}$ slices. Statistical differences were tested using a Mann-Whitney U test (*Cx43*$^{\text{loxP/loxP}}$ vs. *Cx43*$^{\text{TanycyteKO}}$, P=0.0006; n=7 and 7 cells, 6 and 6 mice). *** P<0.001.

(L) Whole-cell current-clamp recording performed in ACSF containing 2,5 mM glucose showing that the bath application of 5 mM lactate has no effect on the spontaneous activity of a POMC neuron from a *Cx43*$^{\text{loxP/loxP}}$; *tdTomato*$^{\text{POMC}}$ mouse.

(M) Firing rate of POMC neurons in *Cx43*$^{loxP/loxP}$; *tdTomato*^{POMC} mice following the bath application of lactate. Statistical differences were tested using a paired Student's t-test (Control vs. Lactate, *P*=0.6042; n=6 cells, 6 mice). ns: non-significant.

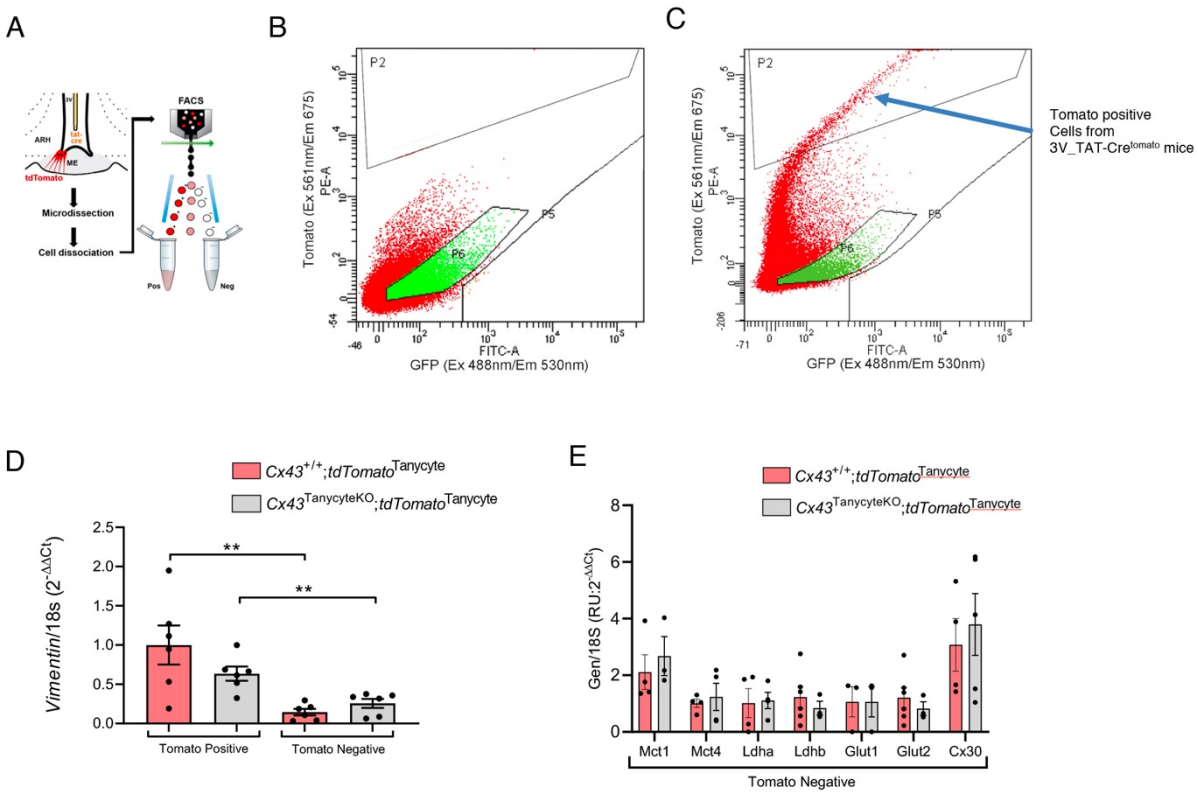


Figure S6. FACS and qPCR analyses in wild-type and mutant mice selectively expressing tdTomato in tanycytes

(A) Schematic model for fluorescence-activated cell sorting (FACS) used to isolate putative Tomato-positive tanycytes in *Cx43*$^{loxP/loxP}$;*tdTomato*$^{loxP\text{-}STOP\text{-}loxP}$ mice injected with TAT-Cre into the third ventricle (3V).

(B-C) Gating strategy for sorting Tomato-positive cells in control (**B**) and Tomato-expressing tissue (**C**).

(D) mRNA expression levels for *Vimentin*, a tanycytic marker, in tdTomato-positive and -negative cells (unpaired Student's t-test; cells Positive vs. Negative for Tomato in *Cx43*$^{+/+}$;*tdTomato* mice, *P*=0.0070; cells Positive vs. Negative for Tomato in *Cx43*^{TanycyteKO};*tdTomato mice*, *P*=0.0056; n=6 mice). ***P*<0.01.

(E) Real-time PCR analysis for various gene transcripts (*Mct1*, *Mct4*, *Ldha*, *Ldhb*, *Glut1*, *Glut4* and *Cx30*) in tdTomato-negative cells from *Cx43*$^{+/+}$;*tdTomato*^{Tanycyte} and *Cx43*^{TanycyteKO};*tdTomato*^{tanycyte} mice (unpaired Student's t-tests; *Mct1*, *P*=0.5679; *Mct4*, *P*=0.6651; *Ldha*, *P*=0.8780; *Ldhb*, *P*=0.5127, *Glut1*, *P*>0.9999; *Glut2*, *P*=0.5127; *Cx30*, *P*=0.6421; n=4 mice).

Figure number	Statistical test	n Number of samples	*P* value
Figure 1C	Wilcoxon matched-pair test (two-tailed)	8 cells, 5 mice (Control) 8 cells, 5 mice (4-CIN)	*P*=0.0078
Figure 1E	Repeated measures one-way ANOVA followed by Tuckey's post hoc test	6 cells, 4 mice (Control) 6 cells, 4 mice (0 Glc) 6 cells, 4 mice (0 Glc + Lactate)	*P*=0.0015 (Control vs. 0 Glc) *P*=0.2007 (Control vs. 0 Glc + Lactate) *P*=0.0280 (O Glc vs. 0 Glc + Lactate)
Figure 1G	Repeated measures one-way ANOVA followed by Tuckey's post hoc test	5 cells, 4 mice (Control) 5 cells, 4 mice (Oxamate) 5 cells, 4 mice (Oxamate+ Lactate)	*P*=0.0008 (Control vs. Oxamate) *P*=0.0004 (Control vs. Oxamate + Lactate) *P*=0.7811 (Oxamate vs. Oxamate + Lactate)
Figure 1I	Repeated measures one-way ANOVA followed by Tuckey's post hoc test	7 cells, 5 mice (Control) 7 cells, 5 mice (Oxamate) 7 cells, 5 mice (Oxamate + Pyruvate)	*P* =0.0277 (Control vs. Oxamate) *P*=0.9561 (Control vs. Oxamate + Pyruvate) *P* =0.0460 (Oxamate vs. Oxamate + Pyruvate)
Figure 1K	Repeated measures one-way ANOVA followed by Tuckey's post hoc test	7 cells, 5 mice (Control) 7 cells, 5 mice (Oxamate POMC neuron) 7 cells, 5 mice (Oxamate POMC neuron + Pyruvate)	*P* =0.0236 (Control vs. Oxamate POMC neuron) *P* =0.9603 (Control vs. Oxamate POMC neruon + Pyruvate) *P* =0.0145 (Oxamate POMC neuron vs. Oxamate POMC neuron + Pyruvate)
Figure 2C	Odinary one-way ANOVA followed by Tuckey's post hoc test	n=6 (Ctrl) n=5 (2-DG) n=6 (4-CIN) n=6 (CBX)	*P*=0.0016 (Ctrl vs 2-DG) *P*=0.0120 (Ctrl vs. 4-CIN) *P*=0.0355 (Ctrl vs. CBX) *P*=0.7092 (2-DG vs. 4-CIN) *P*=0.4239 (2-DG vs. CBX) *P*=0.9558 (4-CIN vs. CBX)
Figure 2D	Odinary one-way ANOVA followed by Tuckey's post hoc test	n=5 (Ctrl) n=5 (2-DG) n=6 (4-CIN) n=6 (CBX)	*P*<0.0001 (Ctrl vs 2-DG) *P*<0.0001 (Ctrl vs. 4-CIN) *P*=0.0009 (Ctrl vs. CBX) *P*<0.0001 (2-DG vs. 4-CIN) *P*<0.0001 (2-DG vs. CBX) *P*=0.6091 (4-CIN vs. CBX)
Figure 2I	Repeated measures one-way ANOVA followed by Tuckey's post hoc test	6 cells, 5 mice (Control + Tanycytic lactate) 6 cells, 5 mice (0 glc + Tanycytic lactate) 6 cells, 5 mice (4-CIN + Tanycytic lactate)	*P*=0.9974 (Control + Tanycytic lactate vs. 0 Glc + Tanycytic lactate) *P*=0.0288 (Control + Tanycytic lactate vs. 4-CIN + Tanycytic lactate) *P*=0.0258 (0 Glc + Tanycytic lactate vs. 4-CIN + Tanycytic lactate)
Figure 2M	Repeated measures one-way ANOVA followed by Tuckey's post hoc test	6 cells, 5 mice (Control) 6 cells, 5 mice (Oxamate Tanycytic) 6 cells, 5 mice (Oxamate tanycytic + lactate)	*P*=0.0143 (Control vs. Oxamate tanycytic) *P*=0.9099 (Control vs. 4-CIN Oxamate tanycytic + Lactate) *P*=0.0474 (Oxamate tanycytic vs. Oxamate tanycytic + Lactate)
Figure 3B	Unpaired Student's t-tests (two-tailed)	5 mice (Tanycyte) 4 mice (POMC neuron)	*Mct1*: *P* =0.0009 (Tanycyte vs. POMC neurons) *Mct2*: *P* =0.0028 (Tanycyte vs. POMC neurons) *Mct4*: *P* =0.0272 (Tanycyte vs. POMC neurons)
Figure 3C	Odinary one-way ANOVA followed by uncorrected Fisher's LSD	4 mice (*Mct1/4*^{TanScramble}) 4 mice (*Mct1/4*^{TanycyteKD})	*P*=0.0231 (*Mct1/4*^{TanScramble} positive cells vs. *Mct1/4*^{TanycyteKD} positive cells) *P*=0.8494 (*Mct1/4*^{TanScramble} negative cells vs. *Mct1/4*^{TanycyteKD} negative cells) *P*=0.0037 (*Mct1/4*^{TanScramble} positive cells vs. *Mct1/4*^{TanScramble} negative cells) *P*=0.0053 (*Mct1/4*^{TanScramble} positive cells vs. *Mct1/4*^{TanycyteKD} negative cells)
Figure 3D	Odinary one-way ANOVA followed by uncorrected Fisher's LSD	4 mice (*Mct1/4*^{TanScramble}) 4 mice (*Mct1/4*^{TanycyteKD})	*P*=0.0320 (*Mct1/4*^{TanScrambld} positive cells vs. *Mct1/4*^{TanycyteKD} positive cells) *P*=0.8944 (*Mct1/4*^{TanScramble} negative cells vs. *Mct1/4*^{TanycyteKD} negative cells) *P*=0.0415 (*Mct1/4*^{TanScramble} positive cells vs. *Mct*1/4^{TanScramble} negative cells) *P*=0.0324 (*Mct1/4*^{TanScramble} positive cells vs. *Mct1/4*^{TanycyteKD} negative cells)

Figure 3G	Mann-Whitney test (two-tailed)	26 cells, 5 mice (*Mct1/4*^{TanScramble}) 26 cells, 5 mice (*Mct1/4*^{TanycyteKD})	*P*=0.0026
Figure 3H	Unpaired Student's t-test (two-tailed)	7 mice (*Mct1/4*^{TanScramble}) 7 mice (*Mct1/4*^{TanycyteKD})	*P*=0.03374
Figure 3I	Two-way ANOVA followed by uncorrected Fisher's LSD test	6 mice (*Mct1/4*^{TanScramble}) 8 mice (*Mct1/4*^{TanycyteKD})	Dark pharse: *P*=0.2454 ; Light phase: *P*=0.8866 ; Mean: *P*=0.360
Figure 3J	Perason correlation	7 mice (*Mct1/4*^{TanScramble}) 7 mice (*Mct1/4*^{TanycyteKD})	*P*=0.0378 (*Mct1/4*^{TanScramble}) *P*=0.5351 (*Mct1/4*^{TanycyteKD})
Figure 3K	Perason correlation	7 mice (*Mct1/4*^{TanScramble}) 7 mice (*Mct1/4*^{TanycyteKD})	*P*=0.0084 (*Mct1/4*^{Scramble}) *P*=0.2553 (*Mct1/4*^{TanycyteKD})
Figure 3L	Two-way ANOVA followed by uncorrected Fisher's LSD test	7 mice (*Mct1/4*^{TanScramble}) 8 mice (*Mct1/4*^{TanycyteKD})	Dark pharse: *P*=0.0012 ; Light phase: *P*=0.3476 ; Mean: *P*=0.0324
Figure 3M	Two-way ANOVA followed by uncorrected Fisher's LSD test	5 mice (*Mct1/4*^{TanScramble}) 7 mice (*Mct1/4*^{TanycyteKD})	Dark pharse: *P*=0.0459 ; Light phase: *P*=0.3042 ;Mean: *P*=0.0037
Figure 3N	Two-way ANOVA followed by uncorrected Fisher's LSD test	5 mice (*Mct1/4*^{TanScramble}) 7 mice (*Mct1/4*^{TanycyteKD})	Dark pharse: *P*=0.0307 ; Light phase: *P*=0.5919 ;Mean: *P*=0.1018
Figure 4C	Wilcoxon matched-pair test (two-tailed)	6 cells, 4 mice (Control) 6 cells, 4 mice (CBX)	*P*=0.0312
Figure 4E	Wilcoxon matched-pair test (two-tailed)	5 cells, 4 mice (Control) 5 cells, 4 mice (CBX + Lactate)	*P*=0.6250
Figure 4G	Unpaired Student's t-tests (two-tailed)	6 mice (*Cx43*$^{+/+}$;*tdTomato*) 6 mice (*Cx43*^{TanycyteKO};*tdTomato)*	*P*=0.0449 (*Cx43*$^{+/+}$;*tdTomato* / Tomato positive vs. *Cx43*^{TanycyteKO};*tdTomato* / Tomato positive) *P*=0.8611 (*Cx43*$^{+/+}$;*tdTomato* /Tomato negative vs. *Cx43*^{TanycyteKO};*tdTomato* /Tomato negative)
Figure 4I	Unpaired Student's t-test (two-tailed)	5 cells, 2 mice (*Cx43*$^{loxP/loxP}$) 10 cells, 4 mice (*Cx43*^{TanycyteKO})	*P*=0.0011
Figure 4L	Mann-Whitney test (two-tailed)	6 cells, 5 mice (*Cx43*$^{loxP/loxP}$; *tdTomato* ^{POMC}) 5 cells, 4 mice (*Cx43*^{TanycyteKO}; *tdTomato* ^{POMC})	*P*=0.0043
Figure 4N	Wilcoxon matched-pair test (two-tailed)	6 cells, 5 mice (*Cx43*^{TanycyteKO}; *tdTomato* ^{POMC} - Control) 6 cells, 5 mice (*Cx43*^{TanycyteKO}; *tdTomato* ^{POMC} - Lactate)	*P*=0.0312
Figure 5C	Two-way ANOVA followed by uncorrected Fisher's LSD test	Basal: 6 mice (*Cx43*$^{loxP/loxP}$) and 10 mice (*Cx43*^{TanycyteKO}) 1 - 4 (Saline): 6 mice (*Cx43*$^{loxP/loxP}$) and 10 mice (*Cx43*^{TanycyteKO}) 1-7 (Glucose 20%): 6 mice (*Cx43*$^{loxP/loxP}$) and 10 mice (*Cx43*^{TanycyteKO})	*P*<0.0001 (Time factor) *P*<0.0001 (Column factor) *P*=0.1326 (Time factor x Column factor)
	Unpaired Student's t-test (two-tailed)	6 mice (*Cx43*$^{loxP/loxP}$) and 10 mice (*Cx43*^{TanycyteKO})	*P*=0.0130
Figure 5D	Unpaired Student's t-tests (two-tailed)	6 mice (*Cx43*$^{+/+}$;*tdTomato*) 6 mice (*Cx43*^{TanycyteKO};*tdTomato*)	*Mct1*: *P*=0.2001 (*Cx43*$^{+/+}$;*tdTomato* vs. *Cx43*^{TanycyteKO};*tdTomato*) *Mct4*: *P*=0.3336 (*Cx43*$^{+/+}$;*tdTomato* vs. *Cx43*^{TanycyteKO};*tdTomato*) *Ldha*: *P*= 0.9195 (*Cx43*$^{+/+}$;*tdTomato* vs. *Cx43*^{TanycyteKO};*tdTomato)* *Ldhb*: *P*=0.0119 (*Cx43*$^{+/+}$;*tdTomato* vs. *Cx43*^{TanycyteKO};*tdTomato*) *Glut1*: *P*=0.9195 (*Cx43*$^{+/+}$;*tdTomato* vs. *Cx43*^{TanycyteKO};*tdTomato*) *Glut2*: *P*=0.0071 (*Cx43*$^{+/+}$;*tdTomato* vs. *Cx43*^{TanycyteKO};*tdTomato*)
Figure 5E	Unpaired Student's t-test (two-tailed)	7 mice (*Cx43*$^{loxP/loxP}$) 9 mice (*Cx43*^{TanycyteKO})	*P*=0.0428

Figure 5F	Paired Student's t-test (two-tailed)	$Cx43^{loxP/loxP}$: 9 mice (day 0) and 9 mice (day 10) $Cx43^{TanycyteKO}$: 9 mice (day 0) and 9 mice (day 10)	P=0.2103 ($Cx43^{loxP/loxP}$/d0 vs. $Cx43^{loxP/loxP}$/d10) P=0.0075 ($Cx43^{TanycyteKO}$/d0 vs. $Cx43^{TanycyteKO}$/d10)
	Unpaired Student's t-test (two-tailed)		P=0.7400 ($Cx43^{loxP/loxP}$/d0 vs. $Cx43^{TanycyteKO}$/d0) P=0.0121 ($Cx43^{loxP/loxP}$/d10 vs. $Cx43^{TanycyteKO}$/d10)
Figure 5G	Unpaired Student's t-test (two-tailed)	8 mice ($Cx43^{loxP/loxP}$) 9 mice ($Cx43^{TanycyteKO}$)	P=0.0287
Figure 5H	Mann-Whitney test (two-tailed)	8 mice ($Cx43^{loxP/loxP}$) 9 mice ($Cx43^{TanycyteKO}$)	P=0.1139
Figure 5I	Two-way ANOVA followed by uncorrected Fisher's LSD test	18h - 17h: 7 mice (before TAT-Cre) and 7 mice (6 days after TAT-Cre)	P<0.0001 (Time factor) P=0.0206 (Column factor) P=0.0001 (Time factor x column factor)
Figure 5J	Two-way ANOVA followed by uncorrected Fisher's LSD test	14h - 13h: 7 mice (before TAT-Cre) and 7 mice (6 days after TAT-Cre)	P<0.0001 (Time factor) P=0.0037 (Column factor) P<0.0001 (Time factor x column factor)
Figure 5K	Two-way ANOVA followed by uncorrected Fisher's LSD test	14h - 13h: 7 mice (before TAT-Cre) and 7 mice (6 days after TAT-Cre)	P<0.0001 (Time factor) P=0.1704 (Column factor) P<0.0001 (Time factor x column factor)
Figure 5L	Two-way ANOVA followed by uncorrected Fisher's LSD test	14h - 13h: 7 mice (before TAT-Cre) and 7 mice (6 days after TAT-Cre)	P<0.0001 (Time factor) P=0.0002 (Column factor) P=0.0147 (Time factor x column factor)
Figure 5M	Unpaired Student's t-tests (two-tailed)	Dark phase: 7 mice (before TAT-Cre) and 7 mice (6 days after TAT-Cre) Light phase: 7 mice (before TAT-Cre) and 7 mice (6 days after TAT-Cre)	Dark phase: P=0.0261 (Before TAT-Cre vs. 6 days after TAT-Cre) Light phase: P=0.0394 (Before TAT-Cre vs. after TAT-Cre)
Figure 5N	Unpaired Student's t-tests (two-tailed)	6 mice ($Cx43^{+/+}$;*tdTomato*) 6 mice ($Cx43^{TanycyteKO}$;*tdTomato*)	*Mct2*: P=0.7581 ($Cx43^{+/+}$;*tdTomato* vs. $Cx43^{TanycyteKO}$;*tdTomato*) *Cartpt*: P=0.4184 ($Cx43^{+/+}$;*tdTomato* vs. $Cx43^{TanycyteKO}$;*tdTomato*) *Pomc*: P= 0.6335 ($Cx43^{+/+}$;*tdTomato* vs. $Cx43^{TanycyteKO}$;*tdTomato*) *Agrp*: P=0.4722 ($Cx43^{+/+}$;*tdTomato* vs. $Cx43^{TanycyteKO}$;*tdTomato*) *Npy*: P=0.0492 ($Cx43^{+/+}$;*tdTomato* vs. $Cx43^{TanycyteKO}$;*tdTomato*)
Figure S2C	Unpaired Student's t-tests (two-tailed)	4 mice (Tomato Positive) 4 mice (Tomato Negative)	*Pomc*: P=0.071 (Tomato Positive vs. Tomato Negative) *Darpp32:* P=0.158 *(Tomato Positive vs. Tomato Negative)* *Gpr50:* P=0.319 *(Tomato Positive vs. Tomato Negative)* *HuC:* P=0.027 *(Tomato Positive vs. Tomato Negative)*
Figure S2F	Unpaired Student's t-tests (two-tailed)	5 mice (GFP Positive) 5 mice (GFP Negative)	*Darpp32*: *P<0.001* (GFP Positive vs. GFP Negative) *Gpr50:* P=0.001 *(GFP Positive vs. GFP Negative)* *Pomc:* P=0.06 *(GFP Positive vs. GFP Negative)* *HuC:* P=0.07 *(GFP Positive vs. GFP Negative)*
Figure S3B	Unpaired Student's t-tests (two-tailed)	7 mice ($Mct2^{POMCScrambled}$) 6 mice ($Mct2^{PomcKD}$)	P=0.0003 (Week 1) P=0.0018 (Week 2) P=0.0045 (Week 3) P=0.0008 (Week 4)

Figure S3C	Unpaired Student's t-tests (two-tailed)	7 mice (*Mct2*^{POMCScrambled}) 6 mice (*Mct2*^{POMCKD})	*P*=0.1135 (Week 1) *P*=0.0534 (Week 2) *P*=0.5188 (Week 3) *P*=0.7470 (Week 4) *P*=0.8773 (Week 5)
Figure S4A	Unpaired Student's t-tests (two-tailed)	4 mice (*Mct1/4*^{TanScramble}) 4 mice (*Mct1/4*^{TanycyteKD})	*P*=0.0200 (*Mct1/4*^{TanScramble} positive cells vs. *Mct1/4*^{TanScramble} negative cells) *P*=0.0134 (*Mct1/4*^{TanycyteKD} positive cells vs. *Mct1/4*^{TanycyteKD} negative cells)
Figure S4B	Unpaired Student's t-tests (two-tailed)	4 mice (*Mct1/4*^{TanScramble}) 4 mice (*Mct1/4*^{TanycyteKD})	*P*=0.0037 (*Mct1/4*^{TanScramble} positive cells vs. *Mct1/4*^{TanScramble} negative cells) *P*=0.0324 (*Mct1/4*^{TanycyteKD} positive cells vs. *Mct1/4*^{TanycyteKD} negative cells)
Figure S4C	Unpaired Student's t-tests (two-tailed)	4 mice (*Mct1/4*^{TanScramble}) 4 mice (*Mct1/4*^{TanycyteKD})	*Mct2*: *P*=0.8204 (*Mct1/4*^{TanScramble} vs. *Mct1/4*^{TanycyteKD}) *Ldha*: *P*=0.5561 (*Mct1/4*^{TanScramble} vs. *Mct1/4*^{TanycyteKD}) *Ldhb*: *P*= 0.5457 (*Mct1/4*^{TanScramble} vs. *Mct1/4*^{TanycyteKD}) *Gck*: *P*=0.1381 (*Mct1/4*^{TanScramble} vs. *Mct1/4*^{TanycyteKD}) *Glut1*: *P*=0.2479 (*Mct1/4*^{TanScramble} vs. *Mct1/4*^{TanycyteKD}) *Glut4*: *P*= 0.9174 (*Mct1/4*^{TanScramble} vs. *Mct1/4*^{TanycyteKD}) *Cx30*: *P*=0.7825 (*Mct1/4*^{TanScramble} vs. *Mct1/4*^{TanycyteKD})
Figure S4D	Two-way ANOVA followed by uncorrected Fisher's LSD test	20h - 19h: 6 *Mct1/4*^{TanScramble} mice and 8 *Mct1/4*^{TanycyteKD} mice	*P*<0.0001 (Time factor) *P*=0.2310 (Column factor) *P*=0.9890 (Time factor x column factor)
Figure S4E	Two-way ANOVA followed by uncorrected Fisher's LSD test	20h - 19h: 7 *Mct1/4*^{TanScramble} mice and 8 *Mct1/4*^{TanycyteKD} mice	*P*<0.0001 (Time factor) *P*=0.2308 (Column factor) *P*=0.3695 (Time factor x column factor)
Figure S4F	Two-way ANOVA followed by uncorrected Fisher's LSD test	20h - 19h: 7 *Mct1/4*^{TanScramble} mice and 8 *Mct1/4*^{TanycyteKD} mice	*P*<0.0001 (Time factor) *P*=0.5215 (Column factor) *P*=0.6883 (Time factor x column factor)
Figure S4G	Two-way ANOVA followed by uncorrected Fisher's LSD test	20h - 19h: 7 *Mct1/4*^{TanScramble} mice and 8 *Mct1/4*^{TanycyteKD} mice	*P*<0.0001 (Time factor) *P*=0.0305 (Column factor) *P*=0.0034 (Time factor x column factor)
Figure S5D	Mann-Whitney test	5 cells, 4 mice (WT) 7 cells, 5 mice (WT+CBX)	P=0.0025
Figure S5K	Mann-Whitney test	7 cells, 6 mice (*Cx43*$^{loxP/loxP}$) 7 cells, 6 mice (*Cx43*^{TanycyteKO})	*P*=0.0006
Figure S5M	Paired Student's t test (two-tailed)	6 cells, 6 mice (*Cx43*$^{loxP/loxP}$; *tdTomato*^{POMC} - Control) 6 cells, 6 mice (*Cx43*$^{loxP/loxP}$; *tdTomato*^{POMC} - Lactate)	*P*=0.6042
Figure S6D	Unpaired Student's t-tests (two-tailed)	6 mice (*Cx43*$^{+/+}$;*tdTomato*) 6 mice (*Cx43*^{TanycyteKO};*tdTomato*)	*P*=0.0070 (*Cx43*$^{+/+}$;*tdTomato* / Tomato Positive vs. *Cx43*$^{+/+}$;*tdTomato* /Tomato Negative) *P*=0.0056 (*Cx43*^{TanycyteKO};*tdTomato* / Tomato Positive vs. *Cx43*^{TanycyteKO};*tdTomato* / Tomato Negative)
Figure S6E	Unpaired Student's t-tests (two-tailed)	6 mice (*Cx43*$^{+/+}$;*tdTomato*) 6 mice (*Cx43*^{TanycyteKO};*tdTomato*)	*Mct1*: *P*=0.5679 (*Cx43*$^{+/+}$;*tdTomato* vs. *Cx43*^{TanycyteKO};*tdTomato*) *Mct4*: *P*=0.6651 (*Cx43*$^{+/+}$;*tdTomato* vs. *Cx43*^{TanycyteKO};*tdTomato*) *Ldha*: *P*= 0.8780 (*Cx43*$^{+/+}$;*tdTomato* vs. *Cx43*^{TanycyteKO};*tdTomato*) *Ldhb*: *P*=0.5127 (*Cx43*$^{+/+}$;*tdTomato* vs. *Cx43*^{TanycyteKO};*tdTomato*) *Glut1*: P>0.9999 (*Cx43*$^{+/+}$;*tdTomato* vs. *Cx43*^{TanycyteKO};*tdTomato*) *Glut2*: *P*=0.5127 (*Cx43*$^{+/+}$;*tdTomato* vs. *Cx43*^{TanycyteKO};*tdTomato*)